Review on Graphene-based Absorbers for Infrared to Ultraviolet Frequencies

Shobhit K. PATEL[1,2,*], *Jaymit SURVE*[3], *Juveriya PARMAR*[2],
Truong Khang NGUYEN[4,5]

[1]Computer Engineering Department Marwadi University, Rajkot, Gujarat, India
[2]Electronics and Communication Engineering Department, Marwadi University,
Rajkot, Gujarat, India
[3]Electrical Engineering Department, Marwadi University,
Rajkot, Gujarat, India
[4]Division of Computational Physics, Institute for Computational Science,
Ton Duc Thang University, Ho Chi Minh City, Vietnam
[5]Faculty of Electrical and Electronics Engineering, Ton Duc Thang University,
Ho Chi Minh City, Vietnam

*Corresponding Author: Shobhit K. PATEL (Email:
shobhitkumar.patel@marwadieducation.edu.in)

Abstract. *The graphene-based absorbers are widely applicable and highly efficient. Graphene has very high electrochemical properties due to which tuning characteristics can be achieved with efficient and broadband absorption response. For this review paper, we have divided the graphene-based absorbers into three categories (Absorber sensors, Solar absorbers, and THz absorbers) based on their applications. We have presented a detailed discussion on various designs and their analysis in this paper. Absorber sensors are mainly applicable in biosensors for the detection of hemoglobin, urine biomolecules using the tuning properties of graphene, and are also applicable in medical, environmental, chemical, biological diagnostic applications. Solar absorbers are applicable in energy harvesting devices. Adding graphene layer in solar absorber design gives the highly efficient and broadband absorption response. THz absorbers are applicable in the THz applications in sensing and imaging devices. Some of the THz absorbers are improving the applications in the new field of nano-optics with 2D material. Graphene and its excellent electrical and optical properties are applied in material designs which create new structures applicable in novel applications like sensing, imaging, solar energy harvesting, etc.*

Keywords

1. Introduction

Day to day usage of electricity is increasing as the human mind is being more and more advance and as the result, fossil fuel consumption is also increasing leading to major environmental issues such as global warming, greenhouse effect, melting of glaciers, etc. To match the increasing energy demand, we need a renewable energy source such as solar energy that is clean, easily convertible to any other energy form, and easily available. We need a flexible and durable

electromagnetic absorber to efficiently use solar energy. These types of absorbers were first introduced by Wood while he invented the surface plasmon resonance (SPR) [1]. Surface plasmon-based near-perfect absorbers piqued a lot of attraction due to their remarkable light trapping abilities and utilization in energy harvesting applications [2]-[5].

Metamaterial which is artificially composed structures has gained remarkable attention due to their extraordinary physical characteristics such as symmetric transmission [6], perfect lens [7], negative refractive index [8], etc. The first metamaterial-based absorber was designed by Landy et al. achieved a near-perfect absorption [9]. These absorbers were mainly fabricated using three layers consisting of a first layer containing a patterned metallic design to achieve the impedance-matching and stop the reflecting light. To act as a resonance cavity and for spacing of electromagnetic waves to disperse the second layer was created of the dielectric layer which was then followed by the metallic plate layer to stop transmission [10]. The only drawback of these absorbers was that the absorption response was of narrowband [11] and a single-peak [12], dual-band [13], or multiband [14] with near-perfect (unity) [15] absorption response was achieved. But we need a highly efficient broadband solar absorber that can absorb the solar energy in most of the wavelength range including terahertz, ultraviolet, visible, infrared, microwave, etc. [16]-[19]. These solar absorbers are utilized in a wide range of applications such as solar energy harvesting, superlenses to optical structure designs [20]-[24].

We can classify the graphene-based absorber in three categories based on their applications in various operating frequency ranges as shown in Fig. 1: 1.) Absorber Sensors, 2.) Solar absorbers, and 3.) THz Absorbers. Absorber sensors are those that achieve single-peak, dual-band, or multi-band absorption response which is near-unity and can be used for sensing applications. Absorber sensors can be used to detect cancer cells. Recent studies also suggest that an absorber sensor can also detect SARS-CoV-2 [25]. Silica and its compounds are widely used for absorber sensor applications due to its remarkably high and solid fluorescence optical characteristics [26]. Gold is also widely used for designing absorber sensors due to its rich material properties i.e., biocompatibility, electro-optical properties, and simple manufacturing and alteration process [27]. Solar absorbers can be defined as absorbers with highly efficient absorption response over a broadband frequency range which should include the ultraviolet, visible, and infrared range and be utilized for the building block of the solar energy harvester. THz absorbers are mostly applicable for polarizers, THz-based photonics devices.

Graphene is a unique, only atom-thick, two-dimensional (2D) element with remarkable electrical, crystal, optical characteristics that can be applied to wide use in a nowadays physics and other related fields [28]. Researchers have proved that a single layer of graphene can absorb 2.3% of white light with 0.1% of refractivity [29]. It is also proved that as the no. of the layer in graphene increases so does the absorption proving the linear relationship [30]. Graphene is also rigid and stable. Nearly several hundred nanometers graphene can also show ballistic transport [31]. Due to these advantages and tunability of graphene, graphene-metasurface-based solar absorbers are in demand. Graphene-based absorber sensors are highly in demand due to their super sensitivity and high range of detection of different biomolecules. Graphene-based optical absorber sensor can detect the single-cell, cell-line, etc. [32]. Graphene gap layers provide increased tunability which improves the sensing in optical absorber sensors [33, 34]. An optical fiber covered by very thin sheet of graphene can be utilized as optical sensor for the detection of minor alteration in the refractive index of the aqueous analyte [35]. Body sweat can also be detected using a graphene-based absorber sensor and humidity sensor. Surface Plasmon resonance (SPR) absorber sensor can be utilized for DNA hybridization [36, 37].

In this review paper, we have analyzed three types of absorbers including absorber sensors, solar absorbers, and THz absorbers. We have analyzed the absorptance response for various designs and compared the results at last. Section 2 contains the designing and modeling part. The third section includes various designs of absorber sensors, solar absorbers, and THz absorbers and

their absorption responses and also includes the discussion of these designs with the comparison table including their applications. Section 4 concludes the paper.

2. Design and analysis

The conductivity σ_s of graphene is derived from Eqs. (1)-(4) [38]

$$\varepsilon(\omega) = 1 + \frac{\sigma_s}{\varepsilon_0 \omega \nabla} \tag{1}$$

$$\sigma_{intra} = \frac{-je^2 k_B T}{\pi \hbar (\omega - j2T)} \left(\frac{\mu_c}{k_B T} + 2 \ln \left(e^{\frac{\mu_c}{k_B T}} + 1 \right) \right) \tag{2}$$

$$\sigma_{inetr} = \frac{-je^2}{4\pi \hbar} \ln \left(\frac{2|\mu_c| - (\omega - j2\Gamma)\hbar}{2|\mu_c| + (\omega - j2\Gamma)\hbar} \right) \tag{3}$$

$$\sigma_s = \sigma_{intra} + \sigma_{inetr} \tag{4}$$

where ε = permittivity; ε_0 = permittivity of vacuum; ω is the angular frequency; ∇ is the thickness of the single-layer sheet of graphene. The conductivity is divided into two segments, intraband conductivity (σ_{intra}), and interband conductivity (σ_{inetr}). Here, k_B is referred to as Boltzmann's constant, $\hbar$ is the decreased plank's constant, T is the room temperature, μ_c is referred to the chemical potential of graphene which is given as $\mu_c = \hbar v_F \sqrt{\pi C V_{DC}/e}$, V_{DC} is the gate voltage, V_F is referred to as Fermi velocity, C stands for capacitance.

The conductivity of graphene σ_s and angle of incidence θ_i are the factors affecting the absorption response of the absorber [39].

$$r(\omega, \theta_i) = \frac{\omega \cos \theta_i \Pi_{00}(\omega, \theta_i)}{2i\hbar ck^2 + \omega \cos \theta_i \Pi_{00}(\omega, \theta_i)} \tag{5}$$

$$\sigma_{||}(\omega, k) = -i \frac{\omega}{4\pi \hbar k^2} \Pi_{00}(\omega, k) \tag{6}$$

$$r(\omega, \theta_i) = \frac{2\pi \cos \theta_i \sigma_{||}(\omega, k)}{c + 2\pi \cos \theta_i \sigma_{||}(\omega, k)} \tag{7}$$

$$\mathcal{R}(\omega, \theta_i) = |r(\omega, \theta_i)|^2 \tag{8}$$

$$\mathcal{R}(\omega, \theta_i) = \tag{9}$$
$$\frac{4\pi^2 \cos^2 \theta_i [\text{Re}^2 \sigma_{||}(\omega, k) + \text{Im}^2 \sigma_{||}(\omega, k)]}{[c + 2\pi \cos \theta_i \text{Re} \sigma_{||}(\omega, k)]^2 + 4\pi^2 \cos^2 \theta_i \text{Im}^2 \sigma_{||}(\omega, k)}$$

$$\mathcal{R}(\omega) = \mathcal{R}(\omega, 0)$$
$$= \frac{4\pi^2 [\text{Re}^2 \sigma(\omega) + \text{Im}^2 \sigma(\omega)]}{[c + 2\pi \text{Re} \sigma(\omega)]^2 + 4\pi^2 \text{Im}^2 \sigma(\omega)} \tag{10}$$

$$A(\omega) = 1 - \mathcal{R}(\omega) - T(\omega) \tag{11}$$

If we consider the transmittance near to zero value then absorption depends only on the reflectance values as shown below.

$$A(\omega) = 1 - \mathcal{R}(\omega) \tag{12}$$

Here, k is the wave vector.

3. Graphene-based absorbers

3.1. Absorber sensors

Absorber sensors are widely used to observe biomolecules which have wide applications in various fields such as medical, environmental, and industrial, etc. [40]-[42]. There are various kinds of absorber sensors are available i.e., optical [43], [44], electrochemical [45], physical [46]. As the optical absorber sensor is compact, low-cost, and due to the utilization of unique nanomaterials it is easy to fabricate. They can be classified into two classes including detection optical absorber sensors and labeled detection absorber sensors [47]. Direct type absorber sensors are cost-effective and SPR based detection is one of the important direct detection absorber sensors as it can be used to detect the biomolecules such as hemoglobin, urine, proteins, etc. [48]-[50]. Taya presented a slab waveguide using air and anisotropic material-based optical sensor for refractometry and sensing-based applications [51, 52, 53]. S A Taya explored the anisotropic left-handed material and results indicated the presence of fundamental mode in the narrow frequency range, increasing positive group velocity with the increment in frequency, and the dispersion curve's important reliance on the anisotropy [54]. Taya et al also presented the

slab waveguide sensor for the detection of cancer cells based on anisotropic left-handed material [55]. Patel et al. reported a highly sensitive and tunable biosensor using phase change material for the detection of hemoglobin biomolecules that achieved the highest sensitivity of 1000 nm/RIU [56]. An environmental analysis can also be carried out using a graphene peptide-based absorber sensor [57]. We can also detect hemoglobin biomolecules with high sensitivity using graphene-based leaky-wave optical absorber sensor design [58]. Raman signals at various combination which is used for the biomedical diagnosis can also be detected using graphene gold nanoribbons substrate in an absorber sensor [59]. Sensitivity is calculated by measuring the difference between the peak of two biomolecules and used as a performance measure for sensors. As the difference between peak increases the quality of sensor is increased due to the improved sensitivity.

Graphene metasurface-based single spit ring resonator and double split-ring resonator SPR absorber sensor

The graphene SPR sensor for the detection of hemoglobin biomolecules is presented in [44]. They have presented two kinds of split-ring resonators one with a single split ring and the other with the double split ring. The design was created using SiO_2 substrate and gold split ring resonator with graphene spacer between substrate and resonator layer. The dimension of the design are as follows: $L = 2.2\,\mu$m, substrate height $H = 0.4\,\mu$m, graphene sheet thickness $= 0.34$ nm, resonator height g $= 200$ nm, radius of inner ring $r_2 = 0.4\,\mu$m, radius of outer ring $r_1 = 0.8\,\mu$m, width of split ring $w = 0.2\,\mu$m. The structure proposed by them is presented in Fig. 1. The voltage (V_g) is given to graphene sheet to control graphene chemical potential (GCP). The graphene surface has also been appointed with the density $J_x = E_x\sigma_s$, $J_y = E_y\sigma_s$. The concentration of hemoglobin and urine is varied in the range of 10 g/l to 40 g/l and 0-1.5 mg/dL to 10 mg/dL for various refractive index values, respectively. The design is investigated using COMSOL Multiphysics.

Absorption analysis has been carried out for the 1.65 μm to 2 μm spectral range as shown in Fig. 2(II). The sensitivity (S) analysis is also carried out given by equation 13 [60]:

$$S = \frac{\Delta\lambda}{\Delta n} \tag{13}$$

where $\Delta\lambda$ is the change in wavelength and Δn is the difference in refractive index. Figure 2(II) shows the relative sensitivity changes in various
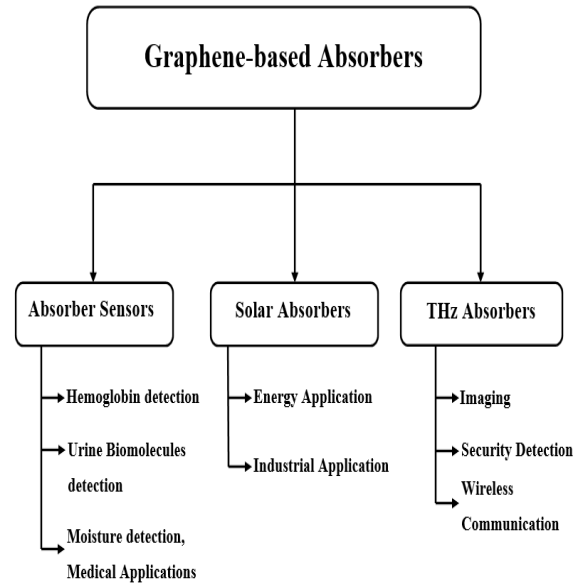

**Fig. 1:** Graphene-based absorbers classification.

concentrations of hemoglobin, urine, and air. The plot illustrates that the two biomolecules from urine and hemoglobin show maximum absorption in 1.5 μm to 2 μm for double split-ring resonator design and 1.65 μm to 2 μm for single split ring resonator design. The achieved highest sensitivities are 1972 nm/RIU for hemoglobin and 1604 nm/RIU for urine biomolecules, where RIU stands for Refractive Index Unit. The highest sensitivities achieved for SSRR structure and DSRR structures are 28785 nm/RIU and 26346 nm/RIU, respectively for hemoglobin-urine concentration. They have also shown the design to be wide-angle sensitive.

Graphene metasurface-based circular and split ring resonator absorber sensor

Parmar et al. reported a graphene-based metasurface design for the detection of urine and hemoglobin biomolecules [61]. A tuning in absorption response is achieved by varying the size and shape of metasurface and graphene chemical potential (GCP). The detailed analysis via varying the physical parameters of design is carried out and results are presented in terms of absorption, electric field, and sensitivity. The design is illustrated in Fig. 3(I) which is designed by taking a gold ground plane and then placing SiO_2 substrate over it followed by a gold resonator separated by a single layer of the graphene sheet. The design parameters are as follows: ground plane thickness, $H_g = 0.5\,\mu$m, sub-
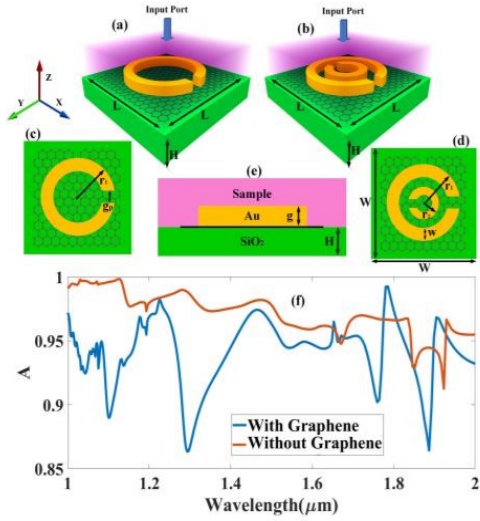
(I)
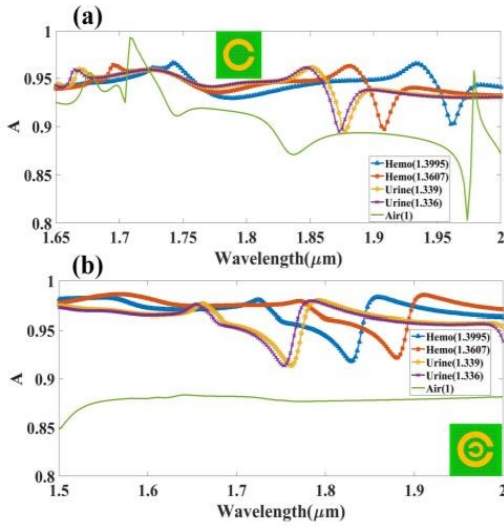
(II)

Fig. 2: Graphene metasurface-based absorber sensors designs and absorption response (I) includes the different views of the graphene-based SSRR and DSRR absorber design such as 3D-view, top view, front view, and the absorption response for two different cases (II) absorption response of (a) SSSR and (b) DSRR for the hemoglobin, urine and air biomolecules (Reprinted with permission taken from [44], 2021, copyright IEEE).

strate height $H_s = 1.5\,\mu$m, graphene sheet height, $H_g = 0.34$ nm, resonator height, $H_r = 0.5\,\mu$m. The length of the structure, L is 7.5 μm. Res-

onator design is varied for radius $R = 2.6\,\mu$m, and $R/2 = 1.3\,\mu$m and corresponding results are presented. The different views of structure including 3D, top, front views are illustrated in Fig. 3(I). The proposed absorber sensor design is simulated using COMSOL Multiphysics with Finite Element Method (FEM). They have considered the periodic boundary conditions over the x and y-axis.

The permittivity and permeability equations of metasurfaces are given in Eqs. (14)-(17). These parameters are obtained from the impedance and the refractive index as given in the Eqs. (14)-(17) [62].

$$Z = \pm\sqrt{\frac{(1 + S_{11})^2 - S_{21}^2}{(1 - S_{11})^2 - S_{21}^2}} \tag{14}$$

$$e^{ink_0 d} = \frac{S_{21}}{1 - S_{11}\frac{Z-1}{Z+1}} \tag{15}$$

$$n = \frac{1}{k_0 d}\left[\left(\left[\ln(e^{ink_0 d})\right]'' + 2m\pi\right) - i\left[\ln(e^{ink_0 d})\right]'\right] \tag{16}$$

$$\varepsilon = \frac{n}{z}, \quad \mu = nz \tag{17}$$

where z is the impedance; S_{11} and S_{21} are reflection and transmission coefficients, respectively; n stands for refractive index; d is referred to unit element's maximum length; k_0 is the wavenumber; m is the branch due to the periodic characteristic of sinusoidal function; μ is the permeability and ε is the permittivity. Figure 3(II) illustrates the absorption response for circular and split ring resonator of radius R for urine concentration ranging from 10 g/l to 60 g/l with the step of 10 g/l for various refractive indices. A large value of the refractive index is required for the maximum absorption. The absorption response is obtained for the wavelength range of 40.7 μm to 41.5 μm.

It is observed that the absorption response shifts to 41.25 μm from 41.15 μm, 41.1 μm from 41 μm for circular resonator and split ring resonator, respectively as seen in Fig. 3 (II) when we increase the refractive index and urine concentration. The absorption response is also investigated by halving the radius of the resonator and is presented in Figs. 3(III) and (IV) for circular and split-ring resonators, respectively. They have also carried out the detailed analysis by comparing two designs by concluding absorption increases when we decrease the radius and wavelength values also decreases for various urine concentrations. The highest
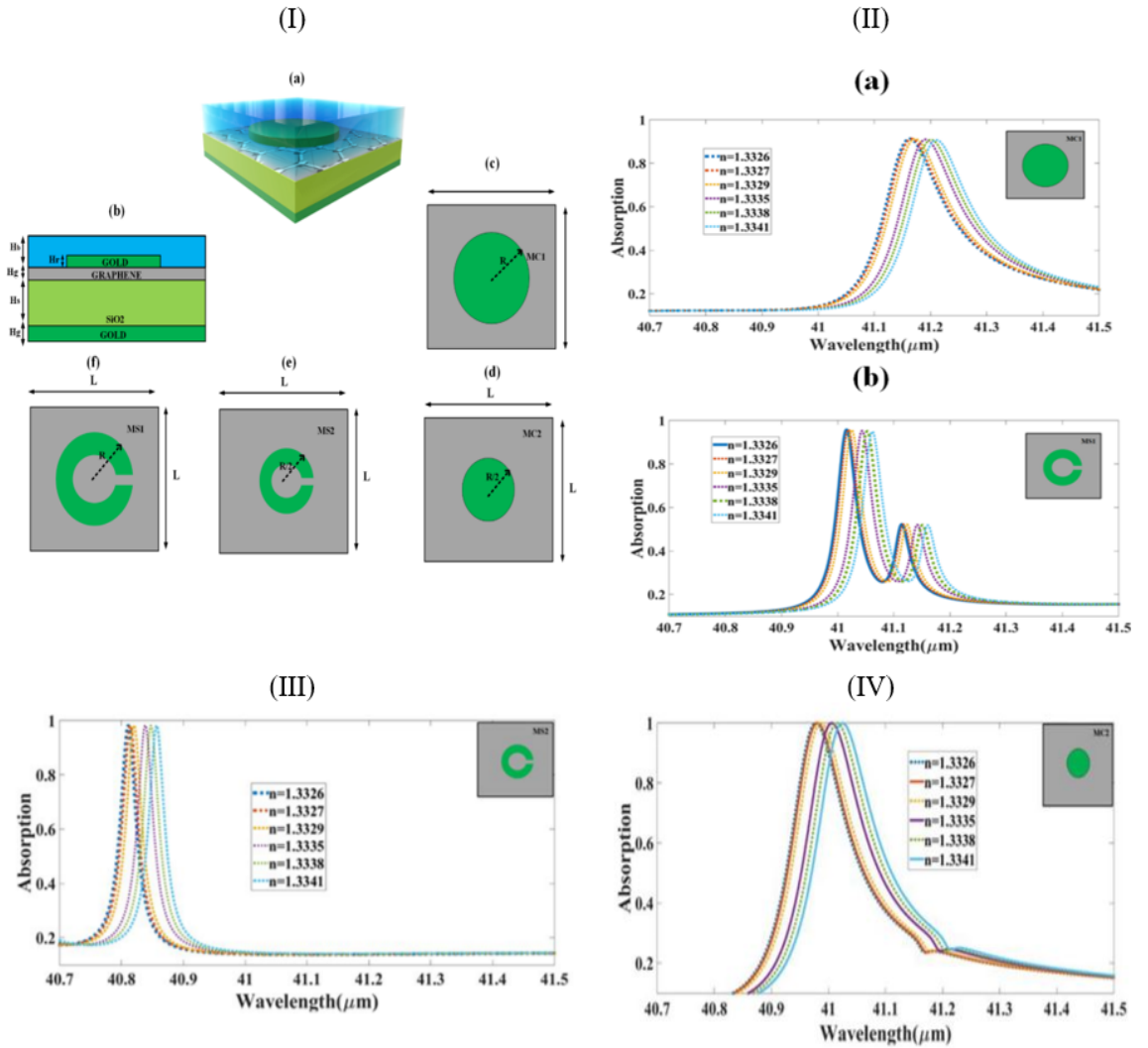
Fig. 3: Graphene metasurface-based circular and split ring resonator absorber sensor design (I) includes the different views of the split ring resonator and circular graphene-based absorber design such as 3D-view, top view, front view (II) absorption response of (a) circular and split ring (b) resonator for different concentration of urine biomolecules for Radius R (III) absorption response of split ring resonator for different concentration of urine biomolecules for Radius $R/2$ (IV) absorption response of split ring resonator for different concentration of urine biomolecules for Radius $R/2$ (Reprinted with permission taken from [61], 2021, copyright Elsevier).

sensitivity of 40000 nm/RIU is obtained for circular metasurface with radius $R/2$.

Graphene-based C-shaped tungsten metasurface refractive index absorber sensor

Patel and co-authors simulated a refractive index absorber sensor with high sensitivity using a C-shaped tungsten metasurface for the infrared region are illustrated in Fig. 4(I) [34]. Refractive index absorber sensors are applicable in medical applications [63, 64]. The design is created by placing a ground plane of tungsten which is followed by a SiO_2 substrate then a tungsten C-shaped resonator is separated from the substrate using a graphene layer sheet. The sensitivity of biosensors depends upon the shift in absorption peak as per the summation of biomolecules over the absorber sensor. The design parameters are as following: length of the structure, $L = 2.2 \ \mu m$, tungsten ground plane height, $B = 0.2$
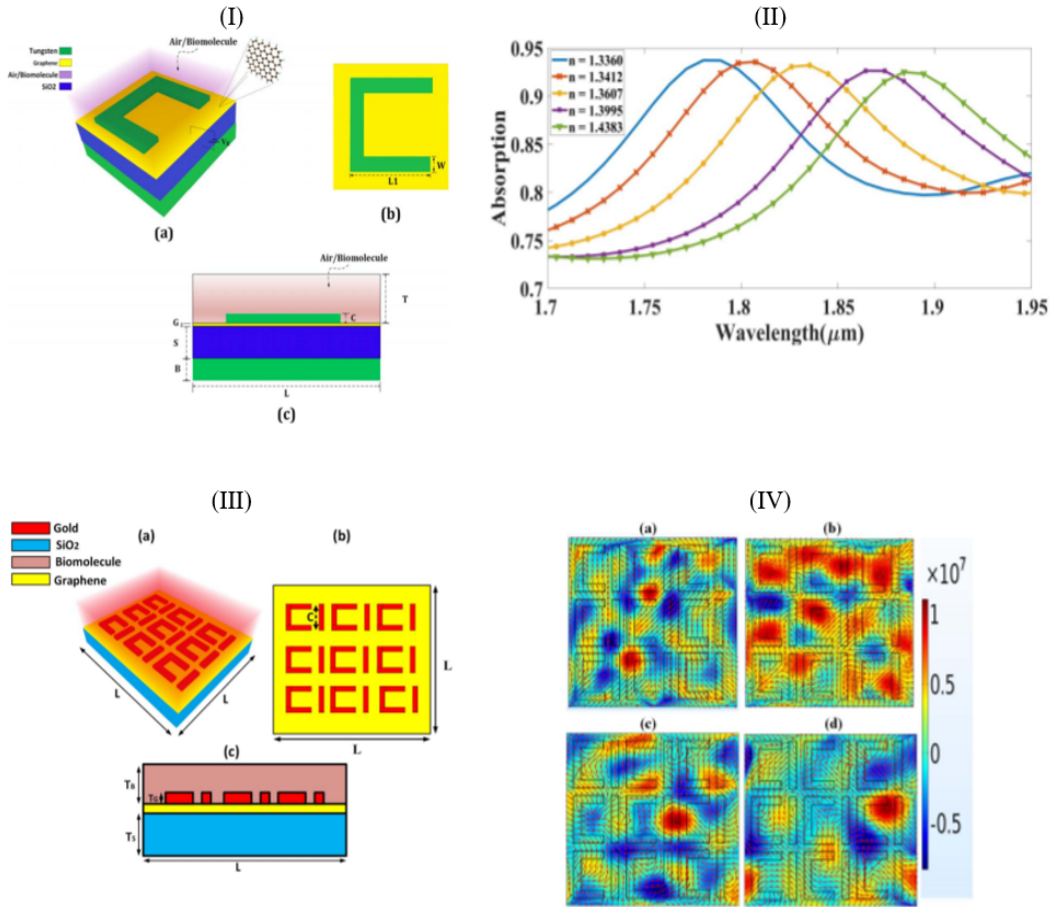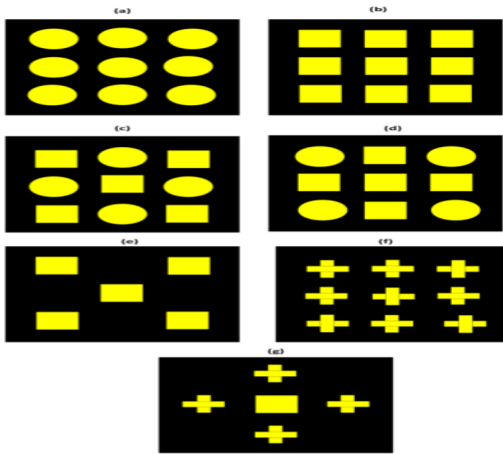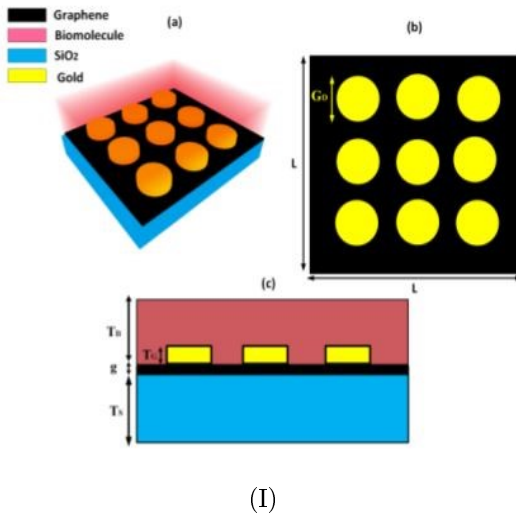
Fig. 4: Graphene-based absorber sensor design (I) graphene-based refractive index absorber sensor using C-shaped tungsten metasurface with (a) 3D, (b) top, (c) front views (II) absorption plot for various compositions of hemoglobin and urine biomolecules for different refractive index (Reprinted with permission from [34], copyright IEEE (III) Graphene-based C-I-shaped array-based refractive index absorber sensor design with (a) 3D, (b) top, (c) front views (IV) Magnetic field density and electric field intensity plots for various values of wavelength including 0.59 μm, 0.76 μm, 0.8 μm, and 0.95 μm, respectively (Reprinted with permission from [65], copyright IEEE).

μm, substrate layer thickness, $S = 0.33$ μm, the C-shaped tungsten resonator having length, $L_1 = 1.6$ μm, width, $W = 0.4$ μm, and the height, $C = 0.30$ nm. The graphene spacer thickness, G, is 0.34 nm. To achieve high absorption, the substrate thickness is set higher than the tungsten ground layer thickness. This shape also helps to trap the waves in the graphene and substrate layer and graphene's high conductivity also helps to achieve high absorption. The detailed analysis is carried out by varying the various parameters and exploring the concerned absorption plot.

The absorption response of the design for various compositions ranging from 10 g/l to 40 g/l with the step of 10 g/l with corresponding refractive index

is shown in Fig. 4(II) for the wavelength range of 1.7 μm to 1.95 μm. The optimized design is also determined by varying various parameters such as substrate height, resonator height, ground layer thickness, etc. from the absorption and reflection plots. This study concludes that the increase in resonator thickness reduces the absorption rate. The same phenomena are observed while increasing the width of the C-shaped resonator. But when we increase the substrate thickness the absorption rate also increases. Fig. 4(II) clearly illustrates the tuning for a different composition, and the shift of 20 nm is observed between hemoglobin molecules with $n = 1.3412$ and urine biomolecules and the high sensitivity of 3846 nm/RIU is achieved for the

(I)

(II)

Fig. 5: Graphene-based refractive index absorber sensor (I) (a) 3D, (b) top, (c) front views of structure (II) variation of the circle, square, and plus shape resonator design for comparative analysis (a) 3×3 circular disk array (b) 3×3 square array (c) circular-square array (d) Square Circular array (e) 2×1×2 square array (f) 3×3 plus-shape array and (g) Plus and square shape array (Reprinted with permission from [67], copyright IEEE).

same. The absorption plot showcases the peak at 1800 nm and 900 nm for hemoglobin and air design, respectively stating the shift of 900 nm with the high sensitivity of 2571 nm/RIU.

Graphene-based C-I shaped array-based refractive index absorber sensor

Patel et al. presented a highly sensitive graphene-based refractive index absorber sensor using arrays of C and I-shaped gold metasurface [65]. The metasurface design is presented in Fig. 4(III). The structure is designed by placing gold C-I shaped arrays over a single layer sheet of graphene which is placed over a substrate of silicon dioxide which is followed by a ground plane of gold material. The design parameters are mentioned here: the length of the structure, $L = 2$ μm, silicon dioxide layer height, $T_S = 0.6$ μm, the height of C-I shaped resonator, $T_G = 0.1$ μm, height of biomolecule layer, $T_B = 1.4$ μm, and the width of C-I shaped resonator, $C = 0.55$ μm. This design is simulated for a different composition of hemoglobin biomolecules ranging in between 10 g/l to 40 g/l with the step of 10 g/l. The analysis is carried out in the wavelength range of 0.2 μm to 1.2 μm and the absorption peak is achieved at 0.73 μm and 0.8 μm indicating the shift of 70 nm for the refractive indices of 1.34 and 1.36 [66] giving the sensitivity of 3500 nm/RIU. The design is also analyzed for variation in physical parameters which indicates the increase in the substrate height increases absorption rate, while the high absorption rate is noted for the low thickness of the ground layer. Fig. 4(IV) illustrate the electric field and magnetic field responsible for the design with a various wavelength which indicates the absorption is low for 0.59 μm and high absorption is achieved for the rest of the wavelength indicated by red color.

Graphene-based refractive index absorber sensor with various combinations of the resonator including circular, square and plus shape arrays

Patel et al. reported a comparative sensitivity analysis of refractive index absorber sensor for various patterns of circle, square, and plus shape resonator as illustrated in Fig. 5 [67]. The metasurface is designed by first placing a substrate of silicon dioxide, followed by an array of gold resonators separated from the substrate by a thin layer of graphene spacer. The hemoglobin biomolecules layer is placed over a gold array resonator. The variation of a different combination of circle, square, and plus-shaped resonator is demonstrated in Fig. 5(II). The design parameters are as follows: length of the structure, $L = 2.5$ μm, silicon dioxide layer height, $T_S = 0.5$ μm, graphene single-layer thickness, g = 0.34 nm, gold array resonator height, $T_G = 0.3$ μm, hemoglobin biomolecule layer thickness, $T_B = 0.6$ μm, and the

diameter of circular disks array resonator, $G_D = 500$ nm. The design is simulated in COMSOL Multiphysics software.

The design is analyzed for various combinations of circular, square, and plus-shaped resonator and concerned absorption responses are presented in Figs. 6(a-e) for the wavelength range of 0.4 μm to 0.55 μm. The absorption responses are achieved for four different compositions of hemoglobin biomolecules ranging between 10 g/l to 40 g/l with the step of 10 g/l and the corresponding refractive indices are also verified experimentally. The 10 nm shift is observed for the hemoglobin molecules for refractive indices of 1.34 RIU and 1.36 RIU giving the sensitivity of 500 nm/RIU. The highest sensitivity is achieved for a 3×3 circular disk array resonator design. While the 3×3 square array, circular-square array, square circular array, 2×1×2 square array, 3×3 plus-shape array, and plus and square shape array achieved the highest sensitivity of 300 nm/RIU, 400 nm/RIU, 300 nm/RIU, 450 nm/RIU, 266 nm/RIU, 400 nm/RIU, respectively. So, the optimized resonator combination of 3×3 circular disk array is achieved and then various physical parameters are varied to observe their effect on absorption response. The comparison is also carried out for air and hemoglobin biomolecules and the 120 nm shift is achieved with the sensitivity of 353 nm/RIU is determined.

3.2. Solar absorber

The fabrication process of metamaterial design is complex due to its three-dimensional designs and losses. Solar absorbers are in demand due to their frequency-dependent resonating response in the ultraviolet, visible, and infrared regions. Metasurface absorbers have remarkable utilization in designing broadband absorbers. We can also add the layer of graphene to achieve broadband absorption. A highly efficient broadband solar absorber can be designed using a monolayer graphene sheet created by a carbon atom positioned in a honeycomb lattice structure [68]. The term broadband absorption emerged due to the coupling of the layers, the broad bandwidth of absorption increases as the no. of layer increases [69, 70]. A specific absorption range can also be attained using the Q-factor during the designing of absorbers and resonators [71]. An absorber must be optically thick but physically thin so that it can achieve a high absorption response [72]. Patel et al. presented a broadband absorber for the visible range using phase change material and the average absorption of 92.86% was achieved

for the frequency range of 500 THz to 740 THz [73].

Graphene-based broadband solar absorber based on C-shape rectangular sawtooth metasurface

Patel et al. presented a wideband graphene-based solar absorber for the near-infrared range placing a rectangular sawtooth at the outer surface of the C-shape resonator [74]. The design is created by first placing tungsten ground layer which is then followed by a silicon dioxide substrate them tungsten made C-shape resonator and the rectangular sawtooth-shaped resonator is placed at the outer surface of C-shape. The resonator and substrate layer are separated by a monolayer sheet of graphene. The three-dimensional view of the structure is presented in Fig. 7(a). The design parameters are: the length of the structure is 2 μm, the tungsten-made ground layer height is 200 nm, the silicon dioxide-based substrate is 330 nm height, the graphene sheet is of 0.34 nm thickness. The C-shape resonator width, length, and height are 400 nm, 1600 nm, 146 nm, respectively. The length and width of the rectangular sawtooth are set to 0.1 μm, 0.2 μm, respectively. The distance between two consecutive rectangular sawtooth is kept at 0.2 μm. Data related to tungsten is determined by the Drude model [75].

The results in terms of absorption, fermi energy plots, electric and magnetic fields are achieved in the wavelength range of 0.71 μm to 1.1 μm presenting the near-infrared (NIR) region. The detailed analysis by varying the position of the rectangular sawtooth is also carried out and related plots are presented in Fig. 7(b). The results indicate that for only C-shaped resonator the average absorption of 66.7%, resonator with rectangular sawtooth positioned at the inner surface of C-shape achieves the average absorption of 86.6%, and the resonator with rectangular sawtooth positioned at the outer surface of C-shape achieves the highest average absorption of 91.8% in the NIR region. The comparative analysis of two designs one with graphene layer and one without graphene layer clearly indicates that the graphene improves the absorption response by a very high margin. This solar absorber is also angle-insensitive and also polarization-insensitive. Analysis of the design is also carried out by varying the design parameter and optimal design is determined.
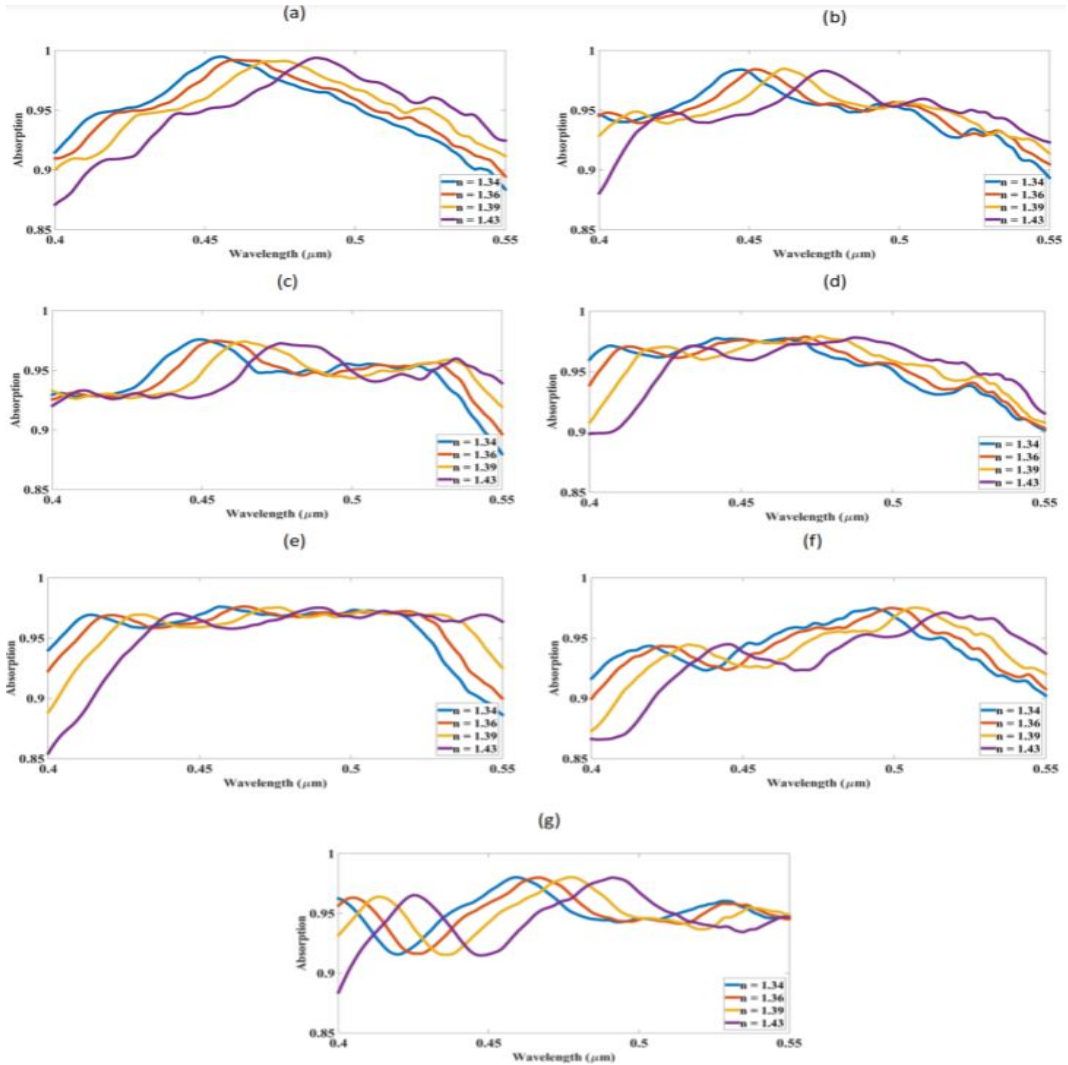
Fig. 6: Absorption response for (a) 3×3 circular disk array (b) 3×3 square array (c) circular-square array (d) Square Circular array (e) 2×1×2 square array (f) 3×3 plus-shape array and (g) Plus and square shape array (Reprinted with permission from [67], copyright IEEE).

Graphene-based broadband solar absorber using uniformly placed gold resonator array

Patel et al. simulated a broadband graphene metasurface-based solar absorber for the NIR regime using a uniformly placed gold resonator array [76]. This paper investigated the effect of the multilayer structure and the pattern of gold resonators on absorption response. This resonator layer is placed over a silicon dioxide substrate layer and these two layers are separated by a single layer of a graphene sheet and below the substrate, there is a ground layer of gold material. They have presented five vari- ous designs by varying the thin square gold resonator pattern and adding these to multilayer substrate of which three variations are illustrated in Figs. 8(a-c). The various geometrical parameters of the designs with the variation for comparative analysis are the height of the gold ground layer, h_g is varied between 80 nm to 120 nm, the substrate height, h_s is varied in the range of 80 nm to 120 nm, too. While the thin square gold resonator thickness, h_l is varied from 30 nm to 70 nm. The reflectance can be given as de- scribed in Eq. (18):

$$R = \left| \frac{Z(\omega) - Z_0(\omega)}{Z(\omega) + Z_0(\omega)} \right| \qquad (18)$$
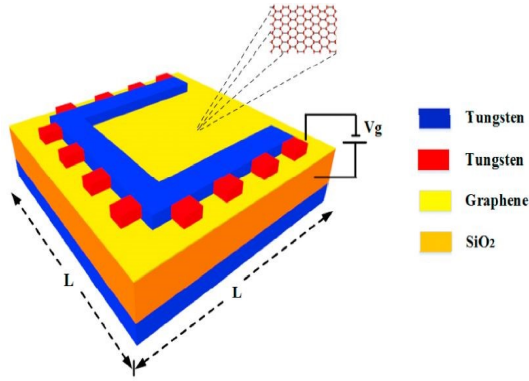
(a)
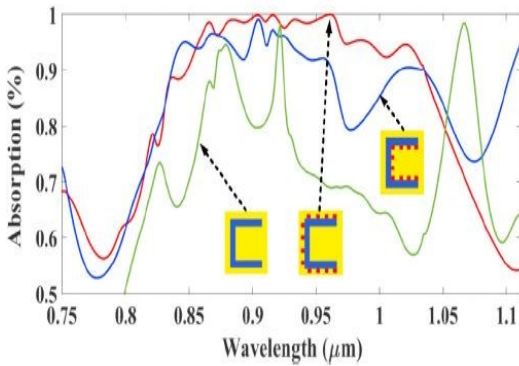
(b)

Fig. 7: Graphene-based wideband solar absorber design (a) 3D view of C-shaped resonator with rectangular sawtooth positioned at the outer surface (b) absorption response of the structure with three different variations C-shaped resonator, resonator with rectangular sawtooth positioned at the inner surface of C-shape, and the resonator with rectangular sawtooth positioned at the outer surface of C-shape achieves the highest average absorption of 91.8% in the NIR region. (Reprinted with the permission from [74], copyright Elsevier).

$$Z(\omega) = \sqrt{\frac{\mu_0 \mu(\omega)}{\varepsilon_0 \varepsilon(\omega)}}, \quad Z_0 = \sqrt{\frac{\mu_0}{\varepsilon_0}} \quad (19)$$

When $Z(\omega)$ and $Z_0(\omega)$ are of same values, the reflectance will be zero, and this is also possible when $\mu(\omega)$ and $\varepsilon(\omega)$ are same. We obtain metamaterials results in the two most important forms of reflection and absorption. The absorption can also be explored using Eqs. (20)-(25) [77]

$$\Delta \times \vec{E} = i\omega\mu_0 \vec{H} \quad (20)$$

$$\Delta \times \vec{E} = -i\omega\varepsilon_0\varepsilon\vec{E} \quad (21)$$

$$A(\omega) = \frac{Q_{abs}(\omega)}{Q_{inc}(\omega)} \quad (22)$$

$$[Q_{abs} = \frac{\omega\varepsilon_0}{2} \int_V \text{Im}[\varepsilon(\omega)]|E|^2 dV \quad (23)$$

$$Q_{inc} = SF(\omega) \quad (24)$$

$$Q_{abs}^{tot} = \int A(\omega)F(\omega)d\omega \quad (25)$$

where Q_{abs} is the power absorbed by the component; Q_{inc} is the power reaching the solar panel from the sun; Q_{abs}^{tot} is total power. A design is also explored using the R-L-C circuit as shown in Fig. 8(d) [78]. Metal induces the resistance R, inductance L, while the capacitance C is caused due to the gap between the metal layer. Eqs. (26)-(28) derives the normalized impedance:

$$Z_1 = j \frac{\omega\mu_0}{\sqrt{\left(\omega\sqrt{\mu_0\varepsilon_S}\right)^2 - k_0^2\sin^2\theta}}$$
$$\times \tan\left(\sqrt{\left(\omega\sqrt{\mu_0\varepsilon_S}\right)^2 - k_0^2\sin^2\theta}\, h_S\right) \quad (26)$$

$$\frac{1}{Z_{in}} = \frac{1}{Z_g} + \frac{1}{Z_m} + \frac{1}{Z_1} \quad (27)$$

$$Z_m \approx \frac{Z_0}{\frac{2\sqrt{n_1}}{T} - (n_1)} \quad (28)$$

where $r = \text{Re}(Z_{in}) - \frac{Z_0}{\text{Re}(Z_{in})} + Z_0$.

The design is simulated using the COMSOL Multiphysics software using the FEM computation method. The results are investigated in the form of absorption, reflectance, and transmittance for the frequency range of 155 THz to 425 THz. From the absorption result, it is clear that the metasurface with two thin square alternate layer checkers array-based design and metasurface with two thin square identical layer checkers array-based design achieved the highest average absorption of 85% in the NIR regime. While metasurface with thin square two identical layers array-based design, metasurface with thin square single layer checkers array-based design, and metasurface with thin square single layer array-based design achieved average absorption of 82%, 72%, and 71%, respectively. The design presented in Fig. 8(c) is then investigated by varying various geometrical
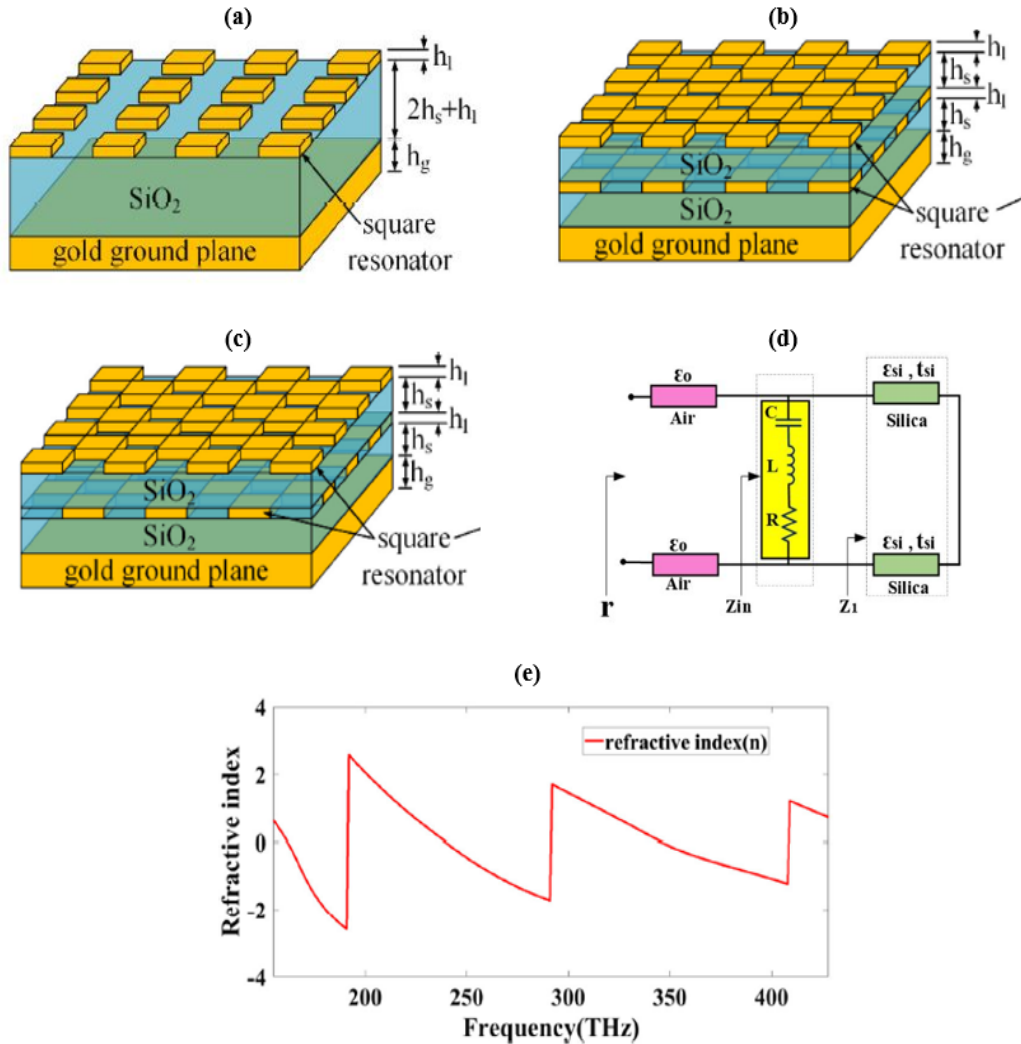
Fig. 8: Graphene-based broadband solar absorber using uniformly positioned thin square gold array-based design (a) basic design (b) metasurface with two thin square identical layer checkers array-based design (c) meta-surface with two thin square alternate layer checkers array-based design (d) Equivalent R-L-C circuit of the implemented design (e) Analysis of refractive index for NIR region (Reprinted with permission from [76], copyright Optica).

parameters to analyze their effect on absorption response as this particular design achieves high average absorption. The optimized parameters for the designs are then determined, where square gold resonator height is 70 nm, substrate height of 120 nm, and gold ground layer thickness is 120 nm. Fig. 8(e) presents the refractive index analysis of the design for 155 THz to 425 THz frequency range and the refractive index is computed by substituting the reflection and transmission coefficients in Eqs. (26)-(28) and Eq. (16). Fig. 8(e) clearly shows the negative refractive index proving the metamaterial

behavior in the whole NIR region. Due to the broadband response of the design, this can be implemented as a unit block for energy harvesting devices.

Graphene-based plus and square shape resonator-based broadband and highly efficient solar absorber

Patel et al. presented a graphene-based plus and square shape resonator-based broadband and highly efficient solar absorber [79]. The design is created by placing silicon dioxide over a ground plane of the

gold layer then a gold resonator of square and silver resonator of plus shape which is separated from a substrate using a thin layer of the graphene sheet. The design's three-dimensional view is presented in Fig. 9(a). The design parameters are: ground plane thickness, $G\_H = 150$ nm, substrate thickness, $S\_H = 150$ nm, graphene sheet height is of 0.34 nm, length and width of the structure is 800 nm, width of gold and silver material resonator, $S\_W = G\_W = 150$ nm, and the resonator thickness, $H = 150$ nm. The proposed structure is simulated using COMSOL Multiphysics software. They have investigated the two variations of the design one where they have added the thin graphene layer and one where it is not added.

The results are presented in form of absorption and reflectance for 200 THz to 1600 THz as illustrated in Figs. 9(b-c). A detailed analysis by varying various physical parameters is also carried out and the related results are illustrated in Figs. 9(d-e). The average absorption of 92.72% and 89.9% is achieved for the design where graphene is present and where it is not present, respectively. The highest average absorption of 97.51% is reported with enhancement in absorption due to the graphene layer positioned above a substrate keeping all the waves inside the substrate layer. The only exception is the ultraviolet region where the average absorption is high for solar absorbers without graphene. The absorption response of these two variations is illustrated in Figs. 9(b-c). The absorption response with respect to variation in gold resonator width and silver resonator width in the range of 150 nm to 250 nm and 100 nm to 200 nm, respectively as illustrated in Figs. 9(d-e). The plot clearly indicates the reduction in absorption response as the width of both the gold and silver resonator increases as it covers more space over the substrate layer increasing the reflectance. The design with graphene sheet achieves the average absorption of 85.48% in infrared, 97.51% in visible, and 89.57% in ultraviolet regime in the frequency range of 200 THz to 1600 THz. An average absorption of 92.72% is achieved for the whole solar spectrum and due to the broadband and high efficiency, it can be used as a unit block for energy harvesting instruments.

Graphene-based L-shape metasurface based wideband solar absorber

Charola et al. reported a tri-layer L-shape metasurface-based wideband solar absorber for the visible and ultraviolet region [80]. The proposed de-

sign is created by metal-dielectric-metal formation, where the L-shape resonator and ground layer are of tungsten material and the substrate is of silicon dioxide as shown in the three-dimensional and front view of the structure illustrated in Fig. 10(a-b). The design is created by placing an L-shaped resonator placed uniformly over a substrate. This design with various top metallic structures is fabricated by scrutinizing the dip-coating techniques reported in [81] and electron beam lithography reported in [82, 83]. The design parameters are: length of the design, $L = 133.33$ nm, ground layer thickness, $B1 = 29$ nm, substrate height, $B2 = 50$ nm, resonator height, $B3 = 20$ nm, length of L-shape, $S = 75$ nm, width of L-shape, $W = 25$ nm, and the distance between consecutive L-shape is set to 58.33 nm.

The design is simulated in COMSOL Multiphysics 5.4 and the results in terms of absorption, the electric field intensity is presented for the frequency range of 340 THz to 1150 THz as illustrated in Fig. 10(c-e). The design achieves an average absorption of 92.2% in visible and 74.1% in the ultraviolet region. The L-shape metallic structure has remarkable capabilities of absorbing, concentrating, and indicating the incoming EM waves in the proper direction for both grazing and oblique incidence. The design is further explored for the effect of variation in physical parameters on absorption response. The effect of change in angle of incidence on absorption response indicates that the design achieves more than 80% average absorption for incidence angle between 0° and 40° as presented in Fig. 10(d). The electric field intensity of the proposed structure at 611 THz is presented in Fig. 10(e).

3.3. THz absorber

THz absorbers are tunable absorbers that are designed in the THz far-infrared frequency range. Furthermore, the terahertz spectrum is full of various applications including wireless communication, security purposes, and imaging applications which all need an efficient absorber that can perfectly absorb the energy from waves [84]-[86]. Tao et al. presented the first-ever THz absorber based on metamaterial which achieved 70% absorption response at 1.3 THz [87].

Graphene gold grating-based THz absorber

Guo et al. reported a hybrid graphene gold grating-based design to obtain improved nonlinear effects in the THz frequency range [88]. The design is presented in Fig. 11(a) with the periodic grating
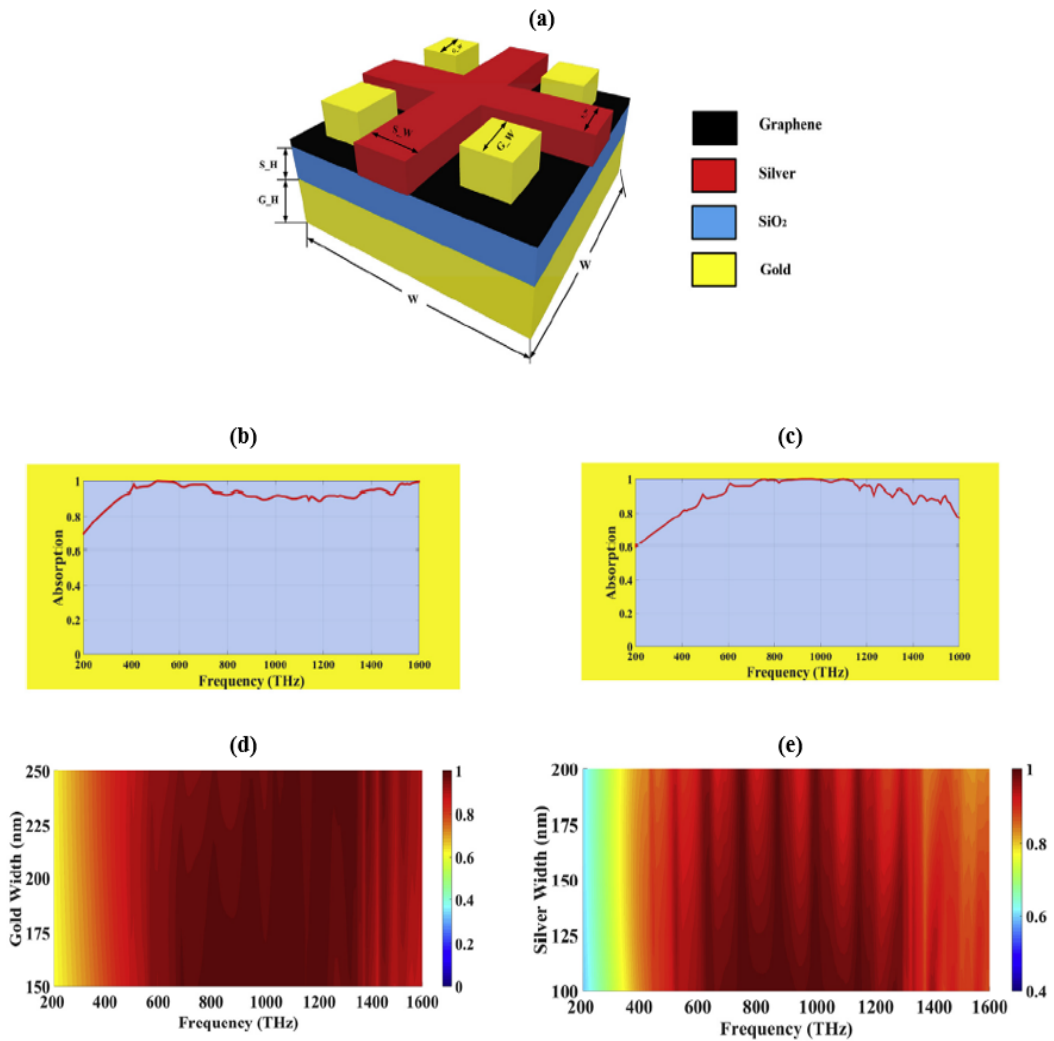
Fig. 9: Graphene-based plus and square resonator-based solar absorber (a) 3D view of the proposed design (b) absorption response of the solar absorber for without adding the single layer of graphene sheet (c) absorption response with single-layer graphene sheet of the solar absorber (d) fermi plot of absorption response for variation of gold resonator width in the range of 150 nm to 250 nm (e) fermi plot for absorption response for variation of silver resonator width in the range of 100 nm to 200 nm (Reprinted with the permission from [79], copyright Elsevier).

in the x-axis direction and with the periodicity of p which is assumed to be expanded to infinity in the y-axis direction. The significant nonlinear response is mostly owing to the localization and intensification of the electric field at the postulated structure's absorption resonance, as well as graphene's large nonlinear conductivity at low THz frequencies. The corresponding absorption results are presented in Fig. 11(b). This design can supposedly be utilized for various applications based on the new nonlinear optics field of 2D material. This can be applied

in THz frequency generators, signal processors, and wave mixers. The suggested hybrid grating's strong field confinement inside nanoscale trenches and along graphene can be exploited to accelerate dipole prohibited transitions on the atomic scale, too [89, 90].

Graphene-based circular array-based absorber
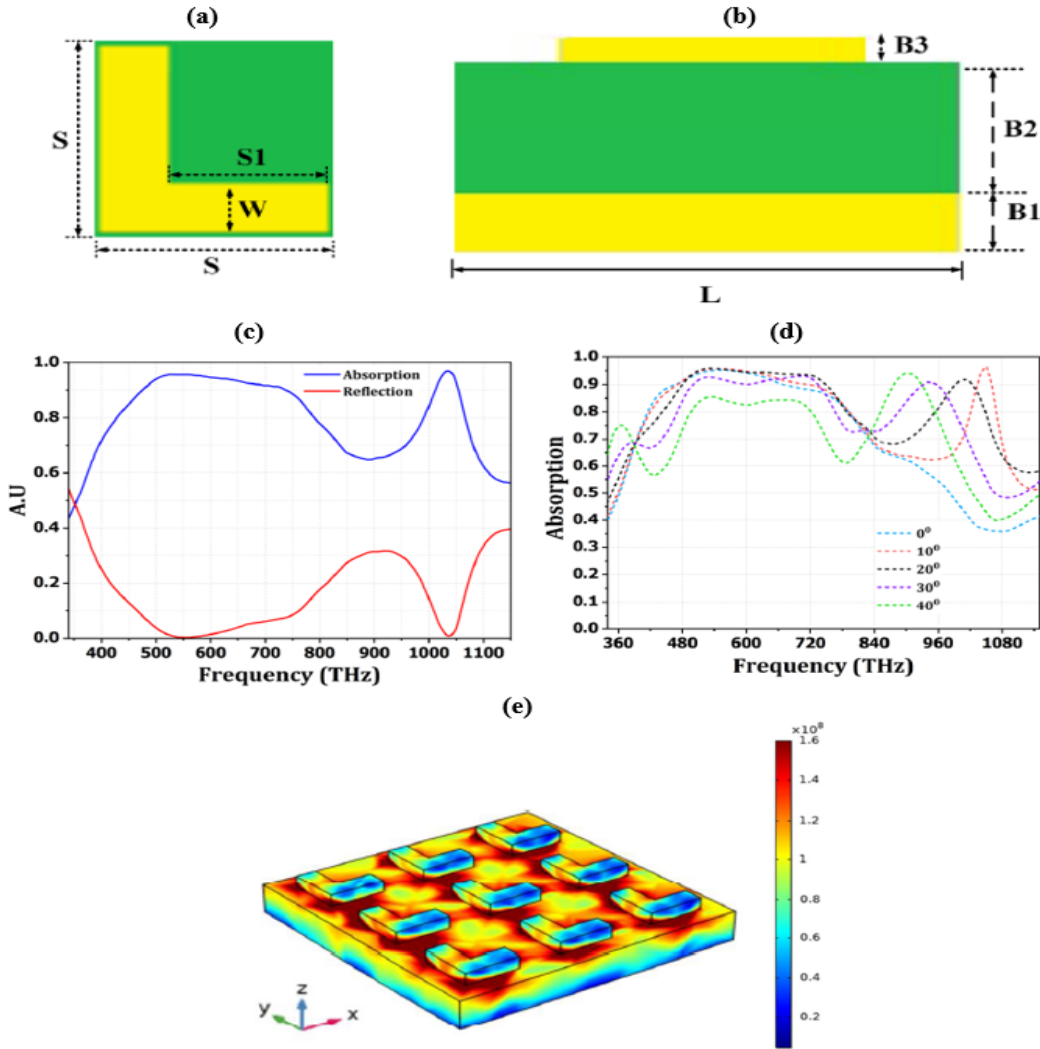
Fig. 10: Graphene-based L-shape metasurface (a) single unit of L with its dimensions (b) top view of the design (c) absorption and reflectance response for 340 THz to 1150 THz (d) absorption response in respect to angle variation for TE waves (e) electric field intensity for 611 THz (Reprinted with permission from [80], copyright Elsevier).

Dave et al. presented a graphene-based circular-array based terahertz absorber for far-infrared (FIR) frequencies [91]. Design is made by a silicon layer and a single layer sheet of graphene and the circular array is positioned as shown in Figs. 12(a-b). A length is set at 7500 nm and height of the design is 1500 nm, the radius of the graphene sheet is 3500 nm, and the gap between the two adjutant circles is 2000 nm. The presented structure is simulated using FEM in COMSOL Multiphysics for the frequency range of 1 THz to 7 THz and the results in form of absorption, reflectance, transmittance, and phase variation. The transmittance coefficient (T_{ij}),

reflectance coefficient (R_{ij}), and phase (ϕ_{ij}) can be defined using Eqs. (29)-(31) [92]

$$T_{ij} = \left| \frac{E_j^{Trans}}{E_i^{Inc}} \right| \ (i, j = x, y) \qquad (29)$$

$$R_{ij} = \left| \frac{E_j^{Reflec}}{E_i^{Inc}} \right| \ (i, j = x, y) \qquad (30)$$

$$\phi_{ij} = arg \left(\frac{E_j^{Trans}}{E_i^{Inc}} \right) \ (i, j = x, y) \qquad (31)$$
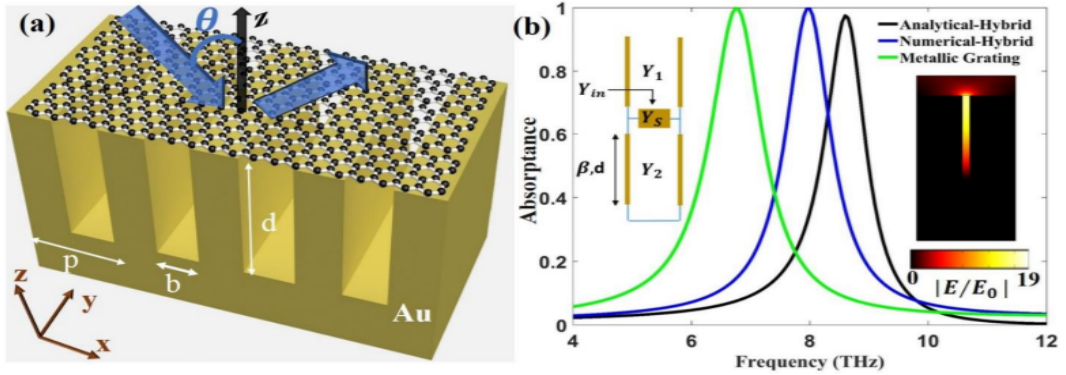
Fig. 11: Graphene gold grating-based THz absorber (a) simplified structure of the design (b) absorption response of the design calculated analytically, and numerically. The absorption response in the green line is of the design where graphene is not applied. (Reprinted with permission from [88], copyright American Physical Society).
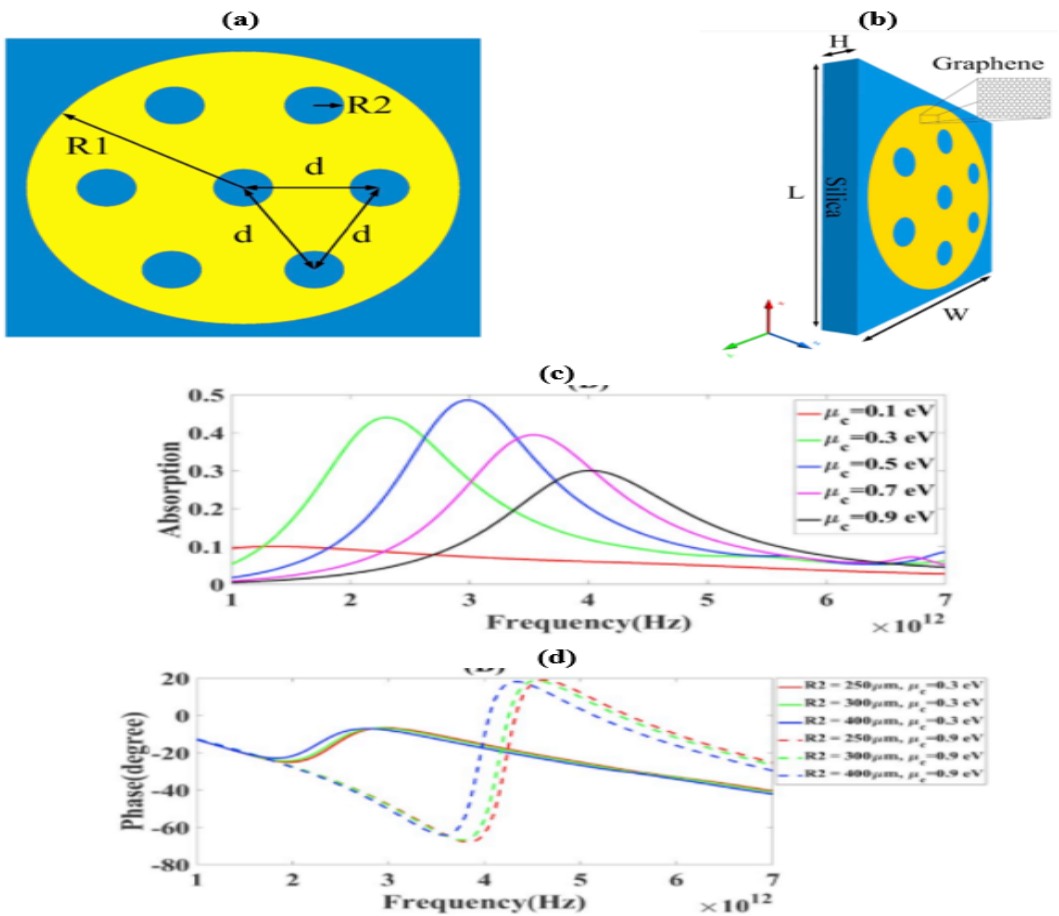
Fig. 12: Graphene-based circular array design (a) Top view of the design illustrating the graphene structure (b) 3D view of design (c) absorption response of the design with respect to variation in GCP (d) achieved tunable phase response for various values of GCP with variation in radius of a small circle (Reprinted with permission from [91], copyright Elsevier).
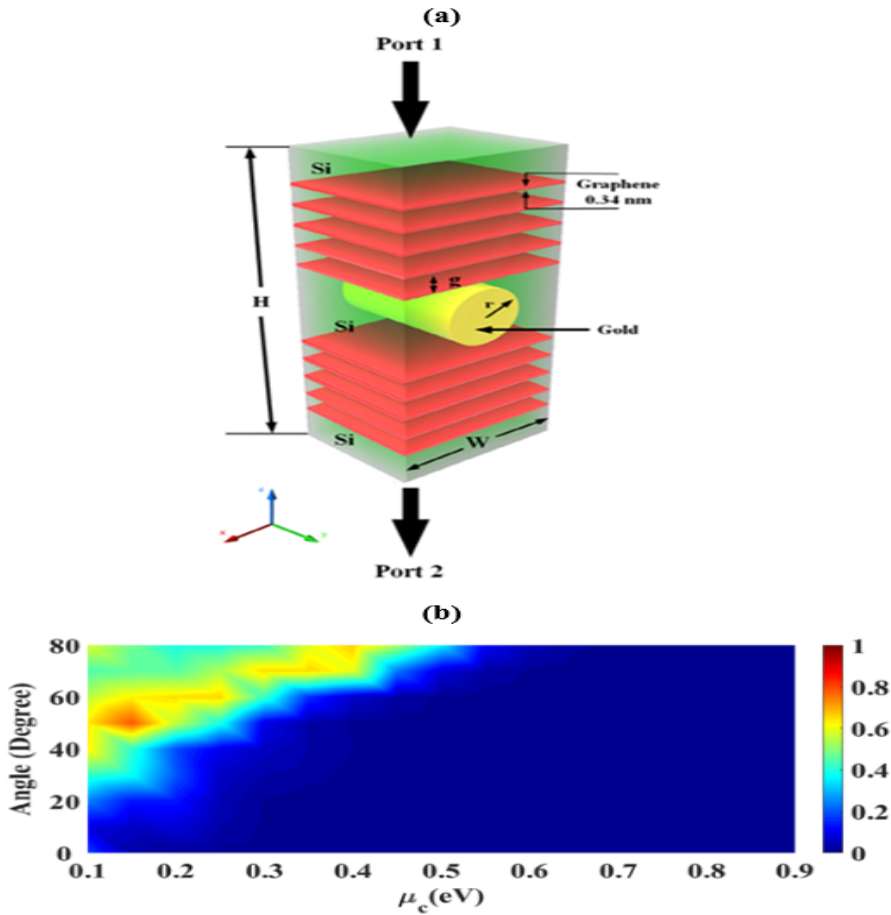
Fig. 13: Multistacked based THz absorber using graphene grating (a) Graphic illustration of the proposed design (b) absorption response with respect to variation in incidence angle and GCP (Reprinted with permission from [93], copyright Wiley).

Results illustrated in Fig. 12(c) indicated the reduction in absorption as the value of graphene chemical potential increases. The plots indicate the change in resonance frequency values as the radius of the smaller circle varies. The phase variation also changes as the GCP and radius of the small circle vary as illustrated in Fig. 12(d). The maximum phase variation of about 85° is observed for the GCP of 0.9 eV. To conclude maximum absorption of 85% is achieved for a smaller circle radius of 250 μm and 450 μm. The tunable ability of this structure can be utilized to design THz sensor, modulator, polarizer, or absorbers.

Tunable multi-stacked-based THz absorber based on graphene-grating

Parmar et al. reported a tunable multi-stacked THz absorber based on graphene grating for the FIR

frequency range [93]. The design of the implemented structure is presented in Fig. 13(a) and we can observe the grating structure formed from gold wires and the stacked graphene layer. In the free space around the gold wire and between two graphene layers silica material is placed. The effective height of the design $H = 1000$ μm, grating structure width $W = 300$ μm, the gap between two graphene layers is 50 μm. In the center of the design a gold circle of radius $r = 50$ μm, is positioned. The absorption, reflectance, and transmittance analysis of the structure is carried out for the frequency range 1 THz to 3 THz. From port 1 the grating structure is excited with transverse magnetic mode. The variation in absorption with respect to incidence angle variation is illustrated in Fig. 13(b). This design can be the unit element of many THz-based applications in sensing and imaging fields.

Tab. 1: Comparison table of absorber sensor with previously published work.

Absorber Sensor Design	Application	Wavelength Range	Sensitivity (nm/RIU)
Single Split Ring Resonator by [44]	Hemoglobin Detection	1.15-1.3 μm	1421
Single Split Ring Resonator by [44]	Urine Detection	1.16-1.19 μm	1604
Double Split Ring Resonator by [44]	Hemoglobin Detection	1.16-1.19 μm	1972
Double Split Ring Resonator by [44]	Urine Detection	1.16-1.19 μm	1595
Single Split Ring Resonator by [44]	Hemoglobin-Urine Detection	-	28785
Double Split Ring Resonator by [44]	Hemoglobin-Urine Detection	-	26346
Circular resonator with radius R by [61]	Urine Detection	40.7-41.5 μm	35000
Circular resonator with radius R/2 by [61]	Urine Detection	40.7-41.5 μm	40000
Split ring resonator with radius R by [61]	Urine Detection	40.7-41.5 μm	33333
Split ring resonator with radius R/2 by [61]	Urine Detection	40.7-41.5 μm	33333
Circular resonator with radius R by [61]	Hemoglobin Detection	40.7-41.5 μm	31000
Split ring resonator with radius R by [61]	Hemoglobin Detection	40.7-41.5 μm	32250
C-shaped tungsten metasurface refractive index absorber sensor by [34]	Hemoglobin-air Detection	1-3 μm	2571
C-shaped tungsten metasurface refractive index absorber sensor by [34]	Hemoglobin-Urine Detection	1.7-1.95 μm	3846
C-I shape array-based design by [65]	Hemoglobin Detection	0.7-0.85 μm	3500
3×3 circular disk array based absorber sensor design by [67]	Hemoglobin Detection	0.4-0.55 μm	500
3×3 square array based absorber sensor design by [67]	Hemoglobin Detection	0.4-0.55 μm	300
Circular square array based absorber sensor design by [67]	Hemoglobin Detection	0.4-0.55 μm	400
Square circular array based absorber sensor design by [67]	Hemoglobin Detection	0.4-0.55 μm	300
2×1 × 2 square array based absorber sensor design by [67]	Hemoglobin Detection	0.4-0.55 μm	450
3×3 plus-shape array based absorber sensor design by [67]	Hemoglobin Detection	0.4-0.55 μm	266
Plus-square shape array based absorber sensor design by [67]	Hemoglobin Detection	0.4-0.55 μm	400
Optical absorber sensor by [94]	Biosensing	1.55-1.58 μm	322
Refractive index absorber sensor design by [95]	Hemoglobin Detection	-	387
Bragg-grating refractive index absorber sensor design by [96]	Sensing	1571.5-1571.8 nm	292
Optical leaky wave absorber sensor by [36]	Biosensing	250-330 THz	431
Optical absorber sensor by [97]	Sensing	0.5-0.75 μm	1139
Photonic crystal-based design by [98]	Biochemical sensing	1.37-1.45 μm	65.7
Slot strip line metamaterial based design by [99]	Biosensor, Slow-light devices, ultrafast-switches	100-240 THz	560
Absorber sensor design by [100]	Biosensor, Slow-light devices, ultrafast-switches	0.9-1.2 μm	294
Refractive index absorber sensor by [101]	Sensing in environmental, chemical, and biological diagnosis	115-215 THz	929
Slot strip based design by [102]	Sensing	380-460 THz	700

In Tab. 1 and Tab. 2 we have compared the absorber sensor and solar absorber with the previously published work.

4.   Conclusion

We have reviewed various recent advances and applications in graphene-based absorbers. Our focus was on the absorber sensors, solar absorbers, and THz absorbers design, result in analysis and their applications. From the result analysis, it is clear that adding the single sheet of monolayer

Tab. 2: Comparison table of solar absorber with previously published work.

Solar absorber design	Frequency/ Wavelength range	% Average absorption (ultraviolet range)	% Average absorption (visible range)	% Average absorption (infrared range)	Angle Insensitive	Polarization Insensitive
C-shape rectangular sawtooth design by [74]	0.81-1.07 μm	-	-	91.8	0° to 80°	Yes
Ref [103]	0.4-0.8 μm	-	71.1	-	0° to 40°	Yes
Ref [104]	100-1200 THz	92.99	86.5	86.1	-	-
Ref [105]	70-130 THz	-	-	90%	-	-
Ref [106]	400-1400 nm	-	Above 90%	Above 90%	-	Yes
Ref [107]	500-900 nm	-	Above 94%	-	0° to 70°	Yes
Ref [108]	400-1400 nm	-	-	-	-	-
Two thin square alternate layer checkers array-based design by [76]	155-425 THz	-	-	85	-	-
Two thin square identical layer checkers array-based design by [76]	155-425 THz	-	-	85	-	-
Ref [109]	537-635 THz	-	70	-	-	-
Ref [110]	450-800 nm	-	80	-	-	-
Plus-square shape resonator design with graphene by [79]	200-1600 THz	89.57	97.51	85.48	-	-
Plus-square shape resonator design with graphene by [79]	200-1600 THz	93.49	92.8	71.84	-	-
Ref [111]	100-1000 THz	92.3	93.7	79.67	-	-
Ref [112]		-	93	-	-	-
Tri-layer L-shape metasurface based by [80]	340-1150 THz	74.1	92.1	-	0° to 30°	-
Four C-shape array metasurface based design by [113]	0.2-0.8 μm	-	92	-	0° to 80°	-
Five circle array metasurface based design by [113]	0.2-0.8 μm	-	91	-	0° to 80°	-
Five C-shape array metasurface based design by [113]	0.2-0.8 μm	-	90	-	0° to 80°	-
Four circle array metasurface based design by [113]	0.2-0.8 μm	-	91	-	0° to 80°	-

graphene improves the absorption response and as we increase the no. of graphene sheets so increases the absorption rate. The absorber sensors are mainly applicable in sensing, imaging applications. They are mainly used as biosensor devices detecting hemoglobin, urine biomolecules. The solar absorbers are mainly applicable as the unit element for the solar energy harvesting devices due to their broadband and highly efficient absorption response which is achieved due to the monolayer graphene sheet. While the THz absorber can be used for many THz-based applications in sensing and imaging. Some of the THz absorbers are applicable in the new field of nonlinear optics field of 2D material. The graphene is also used in absorbers to achieve tuning. So, we can conclude that graphene-based absorbers are widely useful and highly efficient.

References

[1] Wood, R. W. (1902). XLII. On a remarkable case of uneven distribution of light in a diffraction grating spectrum. *The London, Edinburgh, and Dublin Philosophical Magazine and Journal of Science*, 4(21), 396-402.

[2] Li, H., Niu, J., & Wang, G. (2019). Dual-band, polarization-insensitive metamaterial perfect absorber based on monolayer graphene in the mid-infrared range. *Results in Physics*, 13, 102313.

[3] Liang, C., Zhang, Y., Yi, Z., Chen, X., Zhou, Z., Yang, H., ... & Yi, Y. (2019). A broadband and polarization-independent metamaterial perfect absorber with monolayer Cr and Ti elliptical disks array. *Results in Physics*, 15, 102635.

[4] Li, M., Liang, C., Zhang, Y., Yi, Z., Chen, X., Zhou, Z., ... & Yi, Y. (2019). Terahertz wide-band perfect absorber based on open loop with cross nested structure. *Results in Physics*, 15, 102603.

[5] Liu, Z., Tang, P., Liu, X., Yi, Z., Liu, G., Wang, Y., & Liu, M. (2019). Truncated titanium/semiconductor cones for wide-band solar absorbers. *Nanotechnology*, 30(30), 305203.

[6] Wu, S., Xu, S., Zhang, Y., Wu, Y., Jiang, J., Wang, Q., ... & Zhu, Y. (2014). Asymmetric transmission and optical rotation of a quasi-3D asymmetric metallic structure. *Optics letters*, 39(22), 6426-6429.

[7] Pendry, J. B. (2000). Negative refraction makes a perfect lens. *Physical review letters*, 85(18), 3966.

[8] Valentine, J., Zhang, S., Zentgraf, T., Ulin-Avila, E., Genov, D. A., Bartal, G., & Zhang, X. (2008). Three-dimensional optical metamaterial with a negative refractive index. *Nature*, 455(7211), 376-379.

[9] Landy, N. I., Sajuyigbe, S., Mock, J. J., Smith, D. R., & Padilla, W. J. (2008). Perfect metamaterial absorber. *Physical review letters*, 100(20), 207402.

[10] Rhee, J. Y., Yoo, Y. J., Kim, K. W., Kim, Y. J., & Lee, Y. P. (2014). Metamaterial-based perfect absorbers. *Journal of Electromagnetic Waves and Applications*, 28(13), 1541-1580.

[11] Rufangura, P., & Sabah, C. (2015). Dual-band perfect metamaterial absorber for solar cell applications. *Vacuum*, 120, 68-74.

[12] Li, Q., Li, Z., Xiang, X., Wang, T., Yang, H., Wang, X., ... & Gao, J. (2019). Tunable perfect narrow-band absorber based on a metal-dielectric-metal structure. *Coatings*, 9(6), 393.

[13] Wu, P., Chen, Z., Xu, D., Zhang, C., & Jian, R. (2020). A narrow dual-band monolayer unpatterned graphene-based perfect absorber with critical coupling in the near infrared. *Micromachines*, 11(1), 58.

[14] Jiang, L., Yuan, C., Li, Z., Su, J., Yi, Z., Yao, W., ... & Pan, M. (2021). Multi-band and high-sensitivity perfect absorber based on monolayer graphene metamaterial. *Diamond and Related Materials*, 111, 108227.

[15] Mahmud, S., Karim, M., Islam, S. S., Shuvo, M. M. K., Akter, T., Almutairi, A. F., & Islam, M. T. (2021). A multi-band near perfect polarization and angular insensitive metamaterial absorber with a simple octagonal resonator for visible wavelength. *IEEE Access*, 9, 117746-117760.

[16] Shen, X., Cui, T. J., Zhao, J., Ma, H. F., Jiang, W. X., & Li, H. (2011). Polarization-independent wide-angle triple-band metamaterial absorber. *Optics express*, 19(10), 9401-9407.

[17] Bhattacharyya, S., Ghosh, S., Chaurasiya, D., & Srivastava, K. V. (2015). Bandwidth-enhanced dual-band dual-layer polarization-independent ultra-thin metamaterial absorber. *Applied Physics* A, 118(1), 207-215.

[18] Ahir, P., Patel, S. K., Parmar, J., & Katrodiya, D. (2019). Directive and tunable graphene based optical leaky wave radiating structure. *Materials Research Express*, 6(5), 055607.

[19] Gao, R., Xu, Z., Ding, C., Wu, L., & Yao, J. (2015). Graphene metamaterial for multi-band and broadband terahertz absorber. *Optics Communications*, 356, 400-404.

[20] Smith, D. R., Padilla, W. J., Vier, D. C., Nemat-Nasser, S. C., & Schultz, S. (2000). Composite medium with simultaneously negative permeability and permittivity. *Physical review letters*, 84(18), 4184.

[21] Cen, C., Chen, Z., Xu, D., Jiang, L., Chen, X., Yi, Z., ... & Yi, Y. (2020). High quality factor, high sensitivity metamaterial graphene—perfect absorber based on critical coupling theory and impedance matching. *Nanomaterials*, 10(1), 95.

[22] Cen, C., Zhang, Y., Chen, X., Yang, H., Yi, Z., Yao, W., ... & Wu, P. (2020). A dual-band metamaterial absorber for graphene surface plasmon resonance at terahertz frequency. *Physica E: Low-dimensional Systems and Nanostructures*, 117, 113840.

[23] Schurig, D., Mock, J. J., Justice, B. J., Cummer, S. A., Pendry, J. B., Starr, A. F., & Smith, D. R. (2006). Metamaterial electromagnetic cloak at microwave frequencies. *Science*, 314(5801), 977-980.

[24] Ergin, T., Stenger, N., Brenner, P., Pendry, J. B., & Wegener, M. (2010). Three-dimensional invisibility cloak at optical wavelengths. *Science*, 328(5976), 337-339.

[25] Ahmadivand, A., Gerislioglu, B., Ramezani, Z., Kaushik, A., Manickam, P., & Ghoreishi, S. A. (2021). Functionalized terahertz plasmonic metasensors: Femtomolar-level detection of SARS-CoV-2 spike proteins. *Biosensors and Bioelectronics*, 177, 112971.

[26] Ji, X., Wang, H., Song, B., Chu, B., & He, Y. (2018). Silicon nanomaterials for biosensing and bioimaging analysis. *Frontiers in chemistry*, 6, 38.

[27] Holzinger, M., Le Goff, A., & Cosnier, S. (2014). Nanomaterials for biosensing applications: a review. *Frontiers in chemistry*, 2, 63.

[28] Geim, A. K., & Novoselov, K. S. (2010). The rise of graphene. *In Nanoscience and technology: a collection of reviews from nature journals* (pp. 11-19).

[29] Tiwari, S. K., Sahoo, S., Wang, N., & Huczko, A. (2020). Graphene research and their outputs: Status and prospect. *Journal of Science: Advanced Materials and Devices*, 5(1), 10-29.

[30] Flynn, G. W. (2015). Atomic Scale Imaging of the Electronic Structure and Chemistry of Graphene and Its Precursors on Metal Surfaces (No. DOE-Columbia-13937-1). *Columbia Univ., New York, NY (United States)*.

[31] El-Amassi, D. M., & Taya, S. A. (2017). Reflection through a parallel-plate waveguide formed by two graphene sheets. *Photonics and Nanostructures-Fundamentals and Applications*, 24, 53-57.

[32] Li, Z., Zhang, W., & Xing, F. (2019). Graphene optical biosensors. *International journal of molecular sciences*, 20(10), 2461.

[33] Parmar, J., Patel, S. K., Ladumor, M., Sorathiya, V., & Katrodiya, D. (2019). Graphene-silicon hybrid chirped-superstructure bragg gratings for far infrared frequency. *Materials Research Express*, 6(6), 065606.

[34] Patel, S. K., Parmar, J., Kosta, Y. P., Charola, S., Zakaria, R. B., Nguyen, T. K., & Dhasarathan, V. (2020). Graphene-based highly sensitive refractive index biosensors using C-shaped metasurface. *IEEE Sensors Journal*, 20(12), 6359-6366.

[35] Al-Ashi, N. E., Taya, S. A., El-Naggar, S. A., Vigneswaran, D., & Amiri, I. S. (2020). Optical fiber surrounded by a graphene layer as an optical sensor. *Optical and Quantum Electronics*, 52(3), 1-10.

[36] Patel, S. K., Parmar, J., Kosta, Y. P., Ladumor, M., Zakaria, R., Nguyen, T. K., & Dhasarathan, V. (2020). Design of graphene metasurface based sensitive infrared biosensor. *Sensors and Actuators A: Physical*, 301, 111767.

[37] Shushama, K. N., Rana, M. M., Inum, R., & Hossain, M. B. (2017). Graphene coated fiber optic surface plasmon resonance biosensor for the DNA hybridization detection: Simulation analysis. *Optics Communications*, 383, 186-190.

[38] Hanson, G. W. (2008). Dyadic Green's functions and guided surface waves for a surface conductivity model of graphene. *Journal of Applied Physics*, 103(6), 064302.

[39] Parmar, J., Patel, S. K., Katrodiya, D., Nguyen, T. K., Skibina, J. S., & Dhasarathan, V. (2020). Numerical investigation of gold metasurface based broadband near-infrared and near-visible solar absorber. *Physica B: Condensed Matter*, 591, 412248.

[40] Liu, Y., Liu, Y., & Wang, M. (2017). Design, optimization and application of small molecule biosensor in metabolic engineering. *Frontiers in microbiology*, 8, 2012.

[41] Maduraiveeran, G., & Jin, W. (2017). Nanomaterials based electrochemical sensor and biosensor platforms for environmental applications. *Trends in Environmental Analytical Chemistry*, 13, 10-23.

[42] Parmar, J., & Patel, S. K. (2021). Encrypted and tunable graphene-based metasurface refractive index sensor. *Microwave and Optical Technology Letters*.

[43] Ahmadivand, A., Gerislioglu, B., Ahuja, R., & Mishra, Y. K. (2020). Terahertz plasmonics: The rise of toroidal metadevices towards immunobiosensings. *Materials Today*, 32, 108-130.

[44] Patel, S. K., Parmar, J., Sorathiya, V., Zakaria, R., Dhasarathan, V., & Nguyen, T. K. (2021). Graphene-Based Plasmonic Absorber For Biosensing Applications Using Gold Split Ring Resonator Metasurfaces. *Journal of Lightwave Technology*.

[45] Yu, S., & Yi, W. (2007). Single-Walled Carbon Nanotubes as a Chemical Sensor for SO_2 Detection. *IEEE transactions on nanotechnology*, 6(5), 545-548.

[46] Son, K. A., Yang, B., Seo, H. C., Wong, D., Moon, J. S., & Hussain, T. (2017). High-speed graphene field effect transistors on microbial cellulose biomembrane. *IEEE Transactions on Nanotechnology*, 16(2), 239-244.

[47] Shi, X., Zhang, X., Yao, Q., & He, F. (2017). A novel method for the rapid detection of microbes in blood using pleurocidin antimicrobial peptide functionalized piezoelectric sensor. *Journal of microbiological methods*, 133, 69-75.

[48] Gerislioglu, B., Dong, L., Ahmadivand, A., Hu, H., Nordlander, P., & Halas, N. J. (2020). Monolithic metal dimer-on-film structure: New plasmonic properties introduced by the underlying metal. *Nano letters*, 20(3), 2087-2093.

[49] Ahmadivand, A., Gerislioglu, B., Ramezani, Z., & Ghoreishi, S. A. (2019). Attomolar detection of low-molecular weight antibiotics using midinfrared-resonant toroidal plasmonic metachip technology. *Physical Review Applied*, 12(3), 034018.

[50] Ertürk, G., Özen, H., Tümer, M. A., Mattiasson, B., & Denizli, A. (2016). Microcontact imprinting based surface plasmon resonance (SPR) biosensor for real-time and ultrasensitive detection of prostate specific antigen (PSA) from clinical samples. *Sensors and Actuators B: Chemical*, 224, 823-832.

[51] Taya, S. A. (2015). Theoretical investigation of slab waveguide sensor using anisotropic metamaterial. *Optica Applicata*, 45(3).

[52] Taya, S. A. (2014). Slab waveguide with air core layer and anisotropic left-handed material claddings as a sensor. *Opto-Electronics Review*, 22(4), 252-257.

[53] Taya, S. A. (2015). P-polarized surface waves in a slab waveguide with left-handed material for sensing applications. *Journal of Magnetism and Magnetic Materials*, 377, 281-285.

[54] Taya, S. A. (2015). Dispersion properties of lossy, dispersive, and anisotropic left-handed material slab waveguide. *Optik*, 126(14), 1319-1323.

[55] Taya, S. A., Colak, I., Suthar, B., & Ramahi, O. M. (2021). Cancer cell detector based on a slab waveguide of anisotropic, lossy, and dispersive left-handed material. *Applied Optics*, 60(27), 8360-8367.

[56] Patel, S. K., & Parmar, J. (2021). Highly sensitive and tunable refractive index biosensor based on phase change material. *Physica B: Condensed Matter*, 622, 413357.

[57] Wang, L., Zhang, Y., Wu, A., & Wei, G. (2017). Designed graphene-peptide nanocomposites for biosensor applications: A review. Analytica Chimica Acta, 985, 24-40.

[58] Patel, S. K., Parmar, J., Ladumor, M., Ahmed, K., Nguyen, T. K., & Dhasarathan, V. (2020). Numerical simulation of a highly directional optical leaky wave antenna using diamond-shaped graphene perturbations. *Applied optics*, 59(8), 2225-2230.

[59] Zhao, X., Dong, J., Cao, E., Han, Q., Gao, W., Wang, Y., ... & Sun, M. (2019). Plasmon-exciton coupling by hybrids between graphene and gold nanorods vertical array for sensor. *Applied Materials Today*, 14, 166-174.

[60] Homola, J., Koudela, I., & Yee, S. S. (1999). Surface plasmon resonance sensors based on diffraction gratings and prism couplers: sensitivity comparison. *Sensors and Actuators B: Chemical*, 54(1-2), 16-24.

[61] Parmar, J., & Patel, S. K. (2022). Tunable and highly sensitive graphene-based biosensor with circle/split ring resonator metasurface for sensing hemoglobin/urine biomolecules. *Physica B: Condensed Matter*, 624, 413399.

[62] Numan, A. B., & Sharawi, M. S. (2013). Extraction of material parameters for metamaterials using a full-wave simulator [education column]. *IEEE Antennas and Propagation Magazine*, 55(5), 202-211.

[63] Ayyanar, N., Raja, G. T., Sharma, M., & Kumar, D. S. (2018). Photonic crystal fiber-based refractive index sensor for early detection of cancer. *IEEE sensors journal*, 18(17), 7093-7099.

[64] Liang, C., Niu, G., Chen, X., Zhou, Z., Yi, Z., Ye, X., ... & Xiao, S. (2019). Tunable triple-band graphene refractive index sensor with good angle-polarization tolerance. *Optics Communications*, 436, 57-62.

[65] Patel, S. K., Parmar, J., Trivedi, H., Zakaria, R., Nguyen, T. K., & Dhasarathan, V. (2020). Highly sensitive graphene-based refractive index biosensor using gold metasurface array. *IEEE Photonics Technology Letters*, 32(12), 681-684.

[66] Jabin, M. A., Ahmed, K., Rana, M. J., Paul, B. K., Luo, Y., & Vigneswaran, D. (2019). Titanium-coated dual-core D-shaped SPR-based PCF for hemoglobin sensing. *Plasmonics*, 14(6), 1601-1610.

[67] Patel, S. K., Parmar, J., Zakaria, R. B., Sharafali, A., Nguyen, T. K., & Dhasarathan, V. (2020). Sensitivity analysis of metasurface array-based refractive index biosensors. *IEEE Sensors Journal*, 21(2), 1470-1477.

[68] Grigorenko, A. N., Polini, M., & Novoselov, K. S. (2012). Graphene plasmonics. *Nature photonics*, 6(11), 749-758.

[69] Wang, B. X., Wang, L. L., Wang, G. Z., Huang, W. Q., Li, X. F., & Zhai, X. (2013). Theoretical

investigation of broadband and wide-angle terahertz metamaterial absorber. *IEEE Photonics Technology Letters*, 26(2), 111-114.

[70] Badloe, T., Mun, J., & Rho, J. (2017). Metasurfaces-based absorption and reflection control: perfect absorbers and reflectors. *Journal of Nanomaterials*, 2017.

[71] Fernez, N., Burgnies, L., Hao, J., Mismer, C., Ducournau, G., Lippens, D., & Lheurette, É. (2018). Radiative quality factor in thin resonant metamaterial absorbers. *IEEE Transactions on Microwave Theory and Techniques*, 66(4), 1764-1772.

[72] Atwater, H. A., & Polman, A. (2011). Plasmonics for improved photovoltaic devices. Materials for sustainable energy. *A collection of peer-reviewed research and review articles from Nature Publishing Group*, 9(3), 205-213.

[73] Patel, S. K., Charola, S., Kumar, R. S., & Parmar, J. (2022). Broadband polarization-insensitive Jerusalem-shaped metasurface absorber based on phase-change material for the visible region. *Physica B: Condensed Matter*, 624, 413440.

[74] Patel, S. K., Charola, S., Jadeja, R., Nguyen, T. K., & Dhasarathan, V. (2021). Wideband graphene-based near-infrared solar absorber using C-shaped rectangular sawtooth metasurface. *Physica E: Low-dimensional Systems and Nanostructures*, 126, 114493.

[75] Ordal, M. A., Bell, R. J., Alexander, R. W., Newquist, L. A., & Querry, M. R. (1988). Optical properties of Al, Fe, Ti, Ta, W, and Mo at submillimeter wavelengths. *Applied optics*, 27(6), 1203-1209.

[76] Patel, S. K., Parmar, J., Katrodiya, D., Nguyen, T. K., Holdengreber, E., & Dhasarathan, V. (2020). Broadband metamaterial-based near-infrared absorber using an array of uniformly placed gold resonators. *JOSA B*, 37(7), 2163-2170.

[77] Akimov, Y. A., & Koh, W. S. (2010). Resonant and nonresonant plasmonic nanoparticle enhancement for thin-film silicon solar cells. *Nanotechnology*, 21(23), 235201.

[78] Johnson, P. B., & Christy, R. W. (1974). Optical constants of transition metals: Ti, v, cr, mn, fe, co, ni, and pd. *Physical review B*, 9(12), 5056-5070.

[79] Patel, S. K., Charola, S., Jani, C., Ladumor, M., Parmar, J., & Guo, T. (2019). Graphene-based highly efficient and broadband solar absorber. *Optical Materials*, 96, 109330.

[80] Charola, S., Patel, S. K., Dalsaniya, K., Jadeja, R., Nguyen, T. K., & Dhasarathan, V. (2021). Numerical investigation of wideband L-shaped metasurface based solar absorber for visible and ultraviolet region. *Physica B: Condensed Matter*, 601, 412503.

[81] Tagliabue, G., Eghlidi, H., & Poulikakos, D. (2014). Rapid-response low infrared emission broadband ultrathin plasmonic light absorber. *Scientific reports*, 4(1), 1-6.

[82] Cheng, C. W., Abbas, M. N., Chiu, C. W., Lai, K. T., Shih, M. H., & Chang, Y. C. (2012). Wide-angle polarization independent infrared broadband absorbers based on metallic multi-sized disk arrays. *Optics express*, 20(9), 10376-10381.

[83] Aydin, K., Ferry, V. E., Briggs, R. M., & Atwater, H. A. (2011). Broadband polarization-independent resonant light absorption using ultrathin plasmonic super absorbers. *Nature communications*, 2(1), 1-7.

[84] Ferguson, B., & Zhang, X. C. (2002). Materials for terahertz science and technology. *Nature materials*, 1(1), 26-33.

[85] Darmo, J., Tamosiunas, V., Fasching, G., Kröll, J., Unterrainer, K., Beck, M., ... & Debbage, P. (2004). Imaging with a Terahertz quantum cascade laser. *Optics express*, 12(9), 1879-1884.

[86] Federici, J. F., Schulkin, B., Huang, F., Gary, D., Barat, R., Oliveira, F., & Zimdars, D. (2005). THz imaging and sensing for security applications—explosives, weapons and drugs. *Semiconductor Science and Technology*, 20(7), S266.

[87] Tao, H., Bingham, C. M., Strikwerda, A. C., Pilon, D., Shrekenhamer, D., Landy, N. I., ... & Averitt, R. D. (2008). Highly flexible wide angle of incidence terahertz metamaterial absorber: Design, fabrication, and characterization. *Physical review B*, 78(24), 241103.

[88] Guo, T., Jin, B., & Argyropoulos, C. (2019). Hybrid graphene-plasmonic gratings to achieve enhanced nonlinear effects at terahertz frequencies. *Physical Review Applied*, 11(2), 024050.

[89] Rivera, N., Kaminer, I., Zhen, B., Joannopoulos, J. D., & Soljačić, M. (2016). Shrinking light to allow forbidden transitions on the atomic scale. *Science*, 353(6296), 263-269.

[90] Sanders, S., May, A., Alabastri, A., & Manjavacas, A. (2018). Extraordinary enhancement of quadrupolar transitions using nanostructured graphene. *ACS Photonics*, 5(8), 3282-3290.

[91] Dave, V., Sorathiya, V., Guo, T., & Patel, S. K. (2018). Graphene based tunable broadband far-infrared absorber. *Superlattices and Microstructures*, 124, 113-120.

[92] Vasić, B., Jakovljević, M. M., Isić, G., & Gajić, R. (2013). Tunable metamaterials based on split ring resonators and doped graphene. *Applied Physics Letters*, 103(1), 011102.

[93] Parmar, J., Patel, S. K., Ahmed, K., & Dhasarathan, V. (2021). Numerical investigation of tunable multistacked metamaterial-based graphene grating. *Microwave and Optical Technology Letters*, 63(4), 1106-1111.

[94] Sahu, S., Ali, J., Yupapin, P. P., & Singh, G. (2018). Optical biosensor based on a cladding modulated grating waveguide. *Optik*, 166, 103-109.

[95] Sahu, S., Ali, J., Yupapin, P. P., & Singh, G. (2018). Porous silicon based Bragg-grating resonator for refractive index biosensor. *Photonic Sensors*, 8(3), 248-254.

[96] Wang, X., & Madsen, C. K. (2014). Highly sensitive compact refractive index sensor based on phase-shifted sidewall Bragg gratings in slot waveguide. *Applied optics*, 53(1), 96-103.

[97] An, G., Li, S., Cheng, T., Yan, X., Zhang, X., Zhou, X., & Yuan, Z. (2019). Ultra-stable D-shaped optical fiber refractive index sensor with graphene-gold deposited platform. *Plasmonics*, 14(1), 155-163.

[98] Olyaee, S., Najafgholinezhad, S., & Banaei, H. A. (2013). Four-channel label-free photonic crystal biosensor using nanocavity resonators. *Photonic sensors*, 3(3), 231-236.

[99] Vafapour, Z. (2017). Near infrared biosensor based on classical electromagnetically induced reflectance (Cl-EIR) in a planar complementary metamaterial. *Optics Communications*, 387, 1-11.

[100] Wei, Z., Li, X., Zhong, N., Tan, X., Zhang, X., Liu, H., ... & Liang, R. (2017). Analogue electromagnetically induced transparency based on low-loss metamaterial and its application in nanosensor and slow-light device. *Plasmonics*, 12(3), 641-647.

[101] He, X. J., Wang, L., Wang, J. M., Tian, X. H., Jiang, J. X., & Geng, Z. X. (2013). Electromagnetically induced transparency in planar complementary metamaterial for refractive index sensing applications. *Journal of physics D: Applied physics*, 46(36), 365302.

[102] Wan, M., Yuan, S., Dai, K., Song, Y., & Zhou, F. (2015). Electromagnetically induced transparency in a planar complementary metamaterial and its sensing performance. *Optik*, 126(5), 541-544.

[103] Sang, T., Gao, J., Yin, X., Qi, H., Wang, L., & Jiao, H. (2019). Angle-insensitive broadband absorption enhancement of graphene using a multi-grooved metasurface. *Nanoscale research letters*, 14(1), 1-8.

[104] Patel, S. K., Charola, S., Parmar, J., Ladumor, M., Ngo, Q. M., & Dhasarathan, V. (2020). Broadband and efficient graphene solar absorber using periodical array of C-shaped metasurface. *Optical and Quantum Electronics*, 52(5), 1-19.

[105] Huang, H., Xia, H., Xie, W., Guo, Z., Li, H., & Xie, D. (2018). Design of broadband graphene-metamaterial absorbers for permittivity sensing at mid-infrared regions. *Scientific reports*, 8(1), 1-10.

[106] Tian, X., & Li, Z. Y. (2016). Visible-near infrared ultra-broadband polarization-independent metamaterial perfect absorber involving phase-change materials. *Photonics Research*, 4(4), 146-152.

[107] Luo, X., Liu, Z., Cheng, Z., Liu, J., Lin, Q., & Wang, L. (2018). Polarization-insensitive and wide-angle broadband absorption enhancement of molybdenum disulfide in visible regime. *Optics express*, 26(26), 33918-33929.

[108] Xu, H., Hu, L., Lu, Y., Xu, J., & Chen, Y. (2019). Dual-band metamaterial absorbers in the visible and near-infrared regions. *The Journal of Physical Chemistry C*, 123(15), 10028-10033.

[109] Rufangura, P., & Sabah, C. (2017). Graphene-based wideband metamaterial absorber for solar cells application. *Journal of Nanophotonics*, 11(3), 036008.

[110] Liu, B., Tang, C., Chen, J., Xie, N., Tang, H., Zhu, X., & Park, G. S. (2018). Multiband and broadband absorption enhancement of monolayer graphene at optical frequencies from multiple magnetic dipole resonances in metamaterials. *Nanoscale research letters*, 13(1), 1-7.

[111] Patel, S. K., Charola, S., Parmar, J., & Ladumor, M. (2019). Broadband metasurface solar absorber in the visible and near-infrared region. *Materials Research Express*, 6(8), 086213.

[112] Lin, H., Sturmberg, B. C., Lin, K. T., Yang, Y., Zheng, X., Chong, T. K., ... & Jia, B.

(2019). A 90-nm-thick graphene metamaterial for strong and extremely broadband absorption of unpolarized light. *Nature Photonics*, 13(4), 270-276.

[113] Surve, J., Parmar, J., Patel, S. K., & Jadeja, R. (2021). Comparative analysis of metasurface array-based solar absorber for visible region. *Optical and Quantum Electronics*, 53(12), 1-22.

About Authors

Shobhit K. PATEL has done his Ph.D. on Electronics & communication engineering at Charotar University of Science and Technology, Changa, India. He is currently working in the area of photonics, metamaterial, antenna, optics and artificial intelligence. He has published several research papers in high impact SCI journals. He has also filed 7 Indian patents on different novel research done by him. He received DST international travel grant in the year 2014 to present a paper in IEEE APSURSI symposium at Memphis, USA. He also received DST International Travel Grant in the year 2017 to present a paper in PIERS Symposium, NTU, Singapore. He has been named in the list of "top 2% scientist worldwide identified by Stanford university" in 2021. He is currently working on many graphene-based projects and has received funding from SERB, DST, for his research. He has been honored with awards for the achievements in the area of the research field.

Jaymit SURVE received the B.Tech degree in Electrical Engineering from Institute of Infrastructure Technology Research and Management, Ahmedabad and the M.E. degree in Electrical Engineering with specialization in Automatic Control and Robotics from The Maharaja Sayajirao University of Baroda, Vadodara. He has recently joined Marwadi University as a Junior Research Fellow in July, 2021. He is currently doing a multidisciplinary reseach in the field of absorbers, sensors, graphene, robotics and AI based Disaster Management. His research areas are graphene, photonics, solar absorbers, sensors, robotics, artificial intelligence, machine learning, control system.

Juveriya PARMAR received the B.Sc. degree in physics from Saurastra University and the M.Sc. degree in physics from Mar-wadi University. She has recently joined as Graduate Research Assistant at University of NebraskaLincoln, Nebraska- USA. Before joining University of Nebraska, Lincoln, She was Employee of Marwadi University for two years, where she worked in the field of graphene, metamaterials, biosensors, solar absorbers. She is currently working in the field of photonics, electromagnetics, materials, etc. She has published more than 27 SCI articles in international journals.

Truong Khang NGUYEN received the B.S. degree in computational physics from the University of Science, Vietnam National University, Ho Chi Minh City, Vietnam, in 2006, and the M.S. and Ph.D. degrees in electrical and computer engineering from Ajou University, Suwon, South Korea, in 2013. From October 2013 to December 2014, he worked at the Division of Energy Systems Research, Ajou University, as a Postdoctoral Fellow. He is currently an Assistant Director and the Head of Division of Computational Physics at the Institute for Computational Science, Ton Duc Thang University, Ho Chi Minh City, and also a Managing Editor of the Journal of Advanced Engineering and Computation. He has authored or coauthored 70 peer-reviewed ISI journal articles and 40 conference papers. He has written one book chapter in the area of terahertz antenna and led one patent on terahertz stripline antenna. His current research interests include microwave antenna for wireless communication, terahertz antenna for compact and efficient source, nano structures and nano antenna for optical applications, and computational micro/nano fluidics.